

1 **The evolution of the Silver Hills volcanic center, and revised $^{40}\text{Ar}/^{39}\text{Ar}$ geochronology**
2 **of Montserrat, Lesser Antilles, and its place within island arc volcanism**

3

4 **S. J. Hatter¹, M. R. Palmer¹, T. M. Gernon¹, R. N. Taylor¹, P. D. Cole², D. N. Barfod³, and**
5 **M. Coussens¹**

6 ¹School of Ocean and Earth Science, National Oceanography Centre, University of
7 Southampton, European Way, Southampton SO14 3ZH, UK.

8 ²School of Geography, Earth and Environmental Sciences, Plymouth University, Drake Circus,
9 Plymouth PL4 8AA, UK.

10 ³Scottish Universities Environmental Research Centre, Rankine Avenue, Scottish Enterprise
11 Park, East Kilbride G75 0QF, UK.

12

13 Corresponding author: Stuart Hatter (sjh1e13@soton.ac.uk)

14

15 **Key points:**

16 • Mapping of the Silver Hills shows volcanism was dominated by andesite dome growth
17 and collapse

18 • New ages reveal overlap in volcanic activity between the Silver and Centre Hills, and
19 Centre and Soufriere Hills

20 • An older previously unreported stage of Soufrière Hills activity at ~450–290 ka erupted
21 hornblende-orthopyroxene lavas

22

23 **Abstract**

24 **250 word limit**

25 Studying the older volcanic centers on Montserrat, Centre Hills and Silver Hills, may reveal how
26 volcanic activity can change over long time periods (≥ 1 Myr), and whether the recent activity at
27 the Soufrière Hills is typical of volcanism throughout Montserrat's history. Here, we present the
28 first detailed mapping of the Silver Hills, the oldest and arguably least studied volcanic center on
29 Montserrat. Silver Hills volcanism was characterized by a similar style of activity as has been
30 documented at the Centre and Soufrière Hills, which was dominantly andesite lava dome growth
31 and collapse, with accompanying Vulcanian style eruptions. The low explosivity of Silver Hills
32 volcanism may be the result of consistent characteristics of mafic magma mixing, which can
33 inhibit the potential for large explosive eruptions. We also present an updated geochronology of
34 volcanism on Montserrat, by revising existing ages and obtaining new $^{40}\text{Ar}/^{39}\text{Ar}$ dates and
35 palaeomagnetic ages from marine tephra layers. We show that the centers of the Silver, Centre,
36 and Soufrière Hills were active during at least ~ 2.17 – 1.03 Ma, ~ 1.14 – 0.38 Ma, and ~ 0.45 Ma–
37 present, respectively. Combined with timings of volcanism on Basse-Terre, Guadeloupe these
38 ages suggest that ~ 0.5 – 1 Ma is a common lifespan for volcanic centers in the Lesser Antilles.
39 Our new dates identify a previously unrecognized overlap in activity between the different
40 volcanic centers, which appears to be a common phenomenon in island arcs. We also identify an
41 older stage of Soufrière Hills activity ~ 450 – 290 ka characterized by the eruption of hornblende-
42 orthopyroxene-phyric lavas.

43 **1. Introduction**

44 Lava dome growth and collapse is a common process at arc volcanoes, e.g. as observed at
45 Merapi volcano, Indonesia (Andreastuti et al., 2000), Mt St Helens, USA (Hoblitt et al., 1980)
46 and Unzen volcano, Japan (Hoshizumi et al., 1999), but volcanic activity can be highly variable
47 over the lifetime of an individual volcanic edifice (e.g. Hildreth & Lanphere, 1994; Komorowski
48 et al., 2005; Myers et al., 1985; Pioli et al., 2015). This is exemplified in the Lesser Antilles arc,
49 where volcanism is dominated by dome-forming eruptions, but varies in composition and style
50 both between discrete volcanic edifices on individual islands, and during the lifetime of an
51 individual volcano. For example, eruptive activity at volcanic centers on Guadeloupe and
52 Martinique has varied from effusive basaltic lava flows forming shield volcanoes, to andesitic
53 dome eruptions to Plinian eruptions (Germa et al., 2011a, 2011b; Komorowski et al., 2005;
54 Maury et al., 1990; Samper et al., 2007). Understanding what causes these changes in eruption
55 styles is crucial to aiding predictions concerning the long-term behavior of a volcano.

56 Volcanism on Montserrat has been of particular interest since the onset of renewed volcanism at
57 the Soufrière Hills Volcano in 1995. As a consequence, it has become one of the most studied
58 volcanoes on Earth. Since 1995 the eruption has had substantial social and economic impacts on
59 the island, including destroying its capital, Plymouth (Kokelaar, 2002), and so gaining insight
60 into the evolution of volcanic activity at Soufrière Hills through time is of considerable interest.

61 Both marine and terrestrial records show that the style of past Soufrière Hills activity has
62 changed little throughout its known ca. 282 kyr history (e.g. Le Friant et al., 2008; Smith et al.,
63 2007), but it may not necessarily continue to behave in this way. For example, Caricchi et al.
64 (2014) suggest that larger eruptions tend to occur towards the end of a volcano's lifetime, raising
65 the possibility that future Soufrière Hills eruptions may be of higher magnitude. Within this
66 context, it is important to note that Soufrière Hills is the latest in a series of volcanic centers on

67 Montserrat. Thus, study of the extinct volcanoes on Montserrat provides an opportunity to
68 investigate volcanic activity over longer time periods, on the order of ~1 Myr, in order to
69 document possible changes. Here, we provide the first detailed account of the physical
70 volcanology of Montserrat's oldest volcanic center, the Silver Hills, in an attempt to better
71 understand how its activity has evolved through time. We also present supporting data and
72 observations from a marine sediment core **that contains eruption products from Montserrat**, and
73 provide new $^{40}\text{Ar}/^{39}\text{Ar}$ dates for the Silver, Centre and Soufrière Hills to better constrain the
74 timing of volcanic activity, providing an updated chronology of volcanism on the island.

75 **2. Geological Setting**

76 Montserrat is an active volcanic island in the Lesser Antilles Arc, formed from the westward
77 subduction of Atlantic crust beneath the Caribbean plate at a rate of *ca.* 2 cm yr⁻¹ (Minster &
78 Jordan, 1978). Detailed geological mapping of Montserrat was first carried out by Macgregor
79 (1938), who identified seven discrete volcanoes, based on the island's geomorphology. This was
80 revised by Rea (1974), who used K-Ar dates to identify six volcanoes, with different relative
81 ages to those proposed by Macgregor (1938). The K-Ar dates of Rea (1974) indicate that
82 activity on Montserrat began at ~4.3 Ma at Roche's Bluff. However, more recent $^{40}\text{Ar}/^{39}\text{Ar}$
83 dating by Harford et al. (2002) suggests that Montserrat is comprised of only three volcanic
84 centers: Silver Hills (*ca.* 2580–1160 ka), Centre Hills (*ca.* 1021–550 ka) and South Soufrière
85 Hills-Soufrière Hills (*ca.* 282 ka to present; Figure 1a). Of these centers, the Silver Hills is the
86 least studied. It is a deeply eroded volcanic center consisting of two-pyroxene andesite (Rea,
87 1974) with volcanoclastic sequences, debris avalanche deposits and areas of extensive
88 hydrothermal alteration (Harford et al., 2002). The Centre Hills consists of two-pyroxene
89 andesite and hornblende-hypersthene andesite (Rea, 1974) with block-and-ash flow, pumice-and-

90 ash flow, pumice-fall, lahar, fluvial and debris avalanche deposits (Harford et al., 2002). The
91 deposits of the Centre Hills also provide evidence for the largest known eruptions on Montserrat,
92 up to magnitude 5 (Coussens et al., 2017).

93 The earliest identified period of activity at the Soufrière Hills volcanic center began ~280 ka with
94 the eruption of two-pyroxene andesites up until ~130 ka. At ~130 ka a period of mafic
95 volcanism formed the South Soufrière Hills (Harford et al., 2002), with deposits dominated by
96 basaltic to basaltic andesite lava flows with mass-wasting and scoria-fall deposits, and some
97 andesitic fallout (Cassidy et al., 2014; Harford et al., 2002; Rea, 1974). Andesites erupted from
98 Soufrière Hills following ~130 ka exhibit a different mineralogy, changing from two-pyroxene
99 andesites to hypersthene-hornblende andesites (Harford et al., 2002). The largest known
100 eruptions of Soufrière Hills occurred during Episode 2, ~174 ka (Coussens et al., 2017; Harford
101 et al., 2002; Smith et al., 2007). This period of activity produced multiple pumice-rich
102 pyroclastic density current deposits 1–3 m thick and a pumice fall deposit 1 m thick ~3 km from
103 the probable source, providing the only evidence of possible Plinian eruptions from the Soufrière
104 Hills volcano.

105 Currently, the Soufrière Hills comprises a central dome complex surrounded by volcanoclastic
106 deposits, which are andesitic in composition. The dome complex comprises four old domes:
107 Chances Peak (<200 ka), Gages Mountain (151 ± 8 ka), Galway's Mountain (112 ± 18 ka) and
108 Perches Mountain (24 ± 4 ka) (Harford et al., 2002), and a dome within English's Crater created
109 by the recent eruption (1995–2010; Figure 1a). The modern dome covers a fifth older dome,
110 Castle Peak (formed *ca.* 1650 AD) (Young et al., 1996), and has undergone multiple successive
111 growth and collapse phases during the recent eruption. Indeed, the current eruptive phase has
112 been dominated by a combination of Vulcanian explosions, dome growth and dome collapse

113 events (Kokelaar, 2002; Wadge et al., 2014), which is probably characteristic of Soufrière Hills
114 activity over the past ~280 kyr (Rea, 1974; Roobol & Smith, 1998; Smith et al., 2007).

115 Large landslide deposits discovered offshore of Montserrat reveal that Soufrière Hills has
116 undergone multiple flank collapse events (Coussens et al., 2016; Deplus et al., 2001; Le Friant et
117 al., 2004; Lebas et al., 2011). Additionally, a debris avalanche occurred during the recent
118 eruption on 26th December 1997, resulting from dome growth over a hydrothermally weakened
119 sector of the wall of English's crater (Sparks et al., 2002; Voight et al., 2002).

120 **3. Methods**

121 **3.1. Field Work**

122 Field mapping was undertaken in the Silver Hills, Montserrat in May 2014 and 2015 at a scale of
123 1:25000, with samples collected for ⁴⁰Ar/³⁹Ar dating and geochemical analysis. The Silver Hills
124 is highly eroded with a current subaerial area of ~6.5 km². The patchy nature of exposures
125 coupled with the generally limited spatial extent of individual units means that radiometric dates
126 are vital to constrain a stratigraphy for the Silver Hills deposits.

127 **3.2. ⁴⁰Ar/³⁹Ar Dating**

128 Twelve lava and three pumice samples were prepared at the Scottish Universities Environmental
129 Research Centre (SUERC) Argon Isotope Facility (AIF), where they were crushed in a jaw-
130 crusher, sieved in to a 250–500 µm size fraction, leached in 20% HNO₃, and passed through a
131 Frantz magnetic barrier laboratory separator (model LB-1) to separate plagioclase phenocrysts
132 from the groundmass. Plagioclase separates were then leached in 5% HF to remove any glass
133 attached to the crystals. 200 mg and 1 g of clean plagioclase phenocryst separates and
134 groundmass (lavas only), respectively, were then hand-picked for ⁴⁰Ar/³⁹Ar dating.

135 The samples were irradiated for one hour in the Oregon State University reactor, Cd-shielded
136 facility, and analyzed on a GVi instruments ARGUS V multi-collector mass spectrometer using a
137 variable sensitivity faraday collector array in static collection (non-peak hopping) mode (Mark et
138 al., 2009; Sparks et al., 2008) at SUERC AIF. Alder Creek sanidine (1.2056 ± 0.0019 Ma, 1σ)
139 (Renne et al., 2011) was used to monitor ^{39}Ar production and establish neutron flux values (J) for
140 the samples. The reader is directed to Coussens et al. (2017) for more details of the method. The
141 average total system blank for laser extractions, measured between each sample run, was $1.5 \pm$
142 0.7×10^{-15} mol ^{40}Ar , $1.2 \pm 1.3 \times 10^{-17}$ mol ^{39}Ar and $8.5 \pm 3.6 \times 10^{-18}$ mol ^{36}Ar for lava samples,
143 and $1.7 \pm 0.1 \times 10^{-15}$ mol ^{40}Ar , $1.6 \pm 0.5 \times 1.1^{-17}$ mol ^{39}Ar and $1.6 \pm 0.7 \times 10^{-17}$ mol ^{36}Ar for
144 pumice samples. All blank, interference and mass discrimination calculations were performed
145 with the *MassSpec* software package (versions 8.058 and 8.16 for andesite and pumice samples
146 respectively, authored by Al Deino, Berkeley Geochronology Center).

147 Plateau ages, or composite plateau ages for replicated samples, are chosen as the best estimates
148 of the emplacement ages. Accepted plateau ages must be derived from a minimum of three
149 contiguous steps (minimum ^{39}Ar content of each step is $\geq 0.1\%$ of total ^{39}Ar release) which
150 overlap in age within 2σ uncertainty, and contains a minimum of 50% of ^{39}Ar released for the
151 combined steps. The scatter between ages of the steps must be low with a MSWD (mean square
152 weighted deviation) less than the 95% probability cut-off (Wendt & Carl, 1991). Further, the
153 inverse isochron formed by the plateau steps must yield an age indistinguishable from the plateau
154 age at 2σ uncertainty, and the $^{40}\text{Ar}/^{36}\text{Ar}$ of the trapped component composition derived from the
155 inverse isochron must be indistinguishable from the composition of air (298.56 ± 0.61 , 2σ) at the
156 2σ uncertainty level.

157 For fall deposits or ignimbrites, the single crystal approach is used to determine an eruptive age
158 because this allows for discrimination of juvenile crystals and crystals derived from other
159 sources, e.g., xenocrysts or antecrysts, but pumice samples yielded low-K plagioclase that could
160 not be analyzed as single crystals. Instead, a multi-grain, two-step heating approach was adopted
161 to increase signal sizes allowing for more precise measurements. The presence of older
162 xenocrysts in these multi-grain aliquots could bias age results, an effect dependent on the age of
163 the xenocryst and its relative potassium content. To account for this possibility, the experiment
164 was repeated ($n \geq 15$) and the youngest, Gaussian distributed population of ages was calculated
165 from the set of analyses.

166 Each individual gas analysis represents an aliquot of 50-100 single grains, loaded into a 4 mm
167 well in a copper planchette. An initial step at ~0.5 watts of power was used to drive off
168 atmospheric gas and liberate argon from any alteration phases that might be present. A second
169 fusion step at 15 watts of power yielded age information associated with the plagioclase crystals.

170 **3.3. Whole Rock Geochemistry**

171 Nb and Y were analyzed on a VG Plasmaquad PQ2+ ICP-MS multi-element analyzer at the
172 University of Southampton following the method of Coussens et al. (2017), in which 0.05 g of
173 powdered sample is analyzed. Precision is better than 3%.

174 Pb and Nd isotopes were measured from 50 and 200 mg (for pumice and lava samples
175 respectively) of hand-picked rock chips 0.5–1 mm in size. Samples were leached and digested
176 following the method of Cassidy et al. (2012), and Pb was isolated from the matrix using AGX-
177 1x8 200-400 mesh anion exchange resin, following the method of Kamber and Gladu (2009). For
178 Nd, the dissolved samples were first passed through cation columns containing AG50-X8 200-
179 400 mesh resin, then through LN Spec columns (Eichrom Industries, Illinois, USA). Pb and Nd

180 isotopes were measured on a MC-ICP-MS (Neptune) at the University of Southampton. Pb
181 isotopes were corrected for instrumental mass fractionation using the SBL74 double spike
182 (Taylor et al., 2015). SRM NBS981 gave $^{206}\text{Pb}/^{204}\text{Pb} = 16.9400 \pm 0.0023$, $^{207}\text{Pb}/^{204}\text{Pb} = 15.4965$
183 ± 0.0026 and $^{208}\text{Pb}/^{204}\text{Pb} = 36.7124 \pm 0.0076$ on $n = 108$ measurements during the course of this
184 study. Measured values for standard JNdi are $^{143}\text{Nd}/^{144}\text{Nd} = 0.512116 \pm 0.000012$ ($n = 36$).

185 **3.4. Core Sample Acquisition**

186 Samples were analyzed from marine sediment core U1396C, from International Ocean
187 Discovery Program (IODP) Expedition 340. This site is located ~35 km southwest of Montserrat
188 (Figure 1b). The core is 145.92 m long and provides a record extending back ~4.5 Ma
189 (Expedition 340 scientists, 2013). This study investigates the tephra layers deposited in the past
190 ~2.35 Ma (the interval represented by the terrestrial record on Montserrat), which have been
191 sampled for geochemical analysis. These samples have been previously analyzed for Pb isotopes
192 by Palmer et al. (2016).

193 **4. Timing of Montserrat Volcanism**

194 **4.1. Existing $^{40}\text{Ar}/^{39}\text{Ar}$ Dates**

195 The $^{40}\text{Ar}/^{39}\text{Ar}$ ages of Montserrat from previous studies are compiled in Table 1. All of these
196 studies used the same strict criteria outlined above (section 3.2) to determine plateau ages. The
197 ages of Harford et al. (2002) and Brown and Davidson (2008) have been recalculated with
198 modern decay constants and standard ages using the Renne et al. (2010, 2011) optimization
199 model, resulting in slightly increased ages. All ages referenced from these authors are the
200 recalculated ages (see supporting information Table S1 for original and recalculated ages). Here,

201 we review the dates from these previous studies to identify which ages are reliable, and which
202 should be viewed with caution.

203 Harford et al. (2002) obtained ages for all of the Montserrat volcanic centers (Figure 1a; Table
204 1). Some of their ages, however, should be viewed with caution, as either their plateau profiles
205 contain evidence of xenocrystic components or Ar recoil, they have a saddle-shaped plateau
206 typical of lavas with excess argon, or have a MSWD which exceeds the critical 95% confidence
207 level. Of the dates considered reliable, two are from the Centre Hills, six are from the Soufrière
208 Hills, and three are from the South Soufrière Hills, with none from the Silver Hills (Table 1).

209 Five $^{40}\text{Ar}/^{39}\text{Ar}$ ages were acquired for the Silver Hills by Brown and Davidson (2008), in the
210 range of ~1.52–1.40 Ma, but only cover a small area of the Silver Hills center, four of which are
211 part of the same stratigraphic sequence (Figure 2; Table 1). These ages were measured from
212 groundmass (i.e. no xenocrystic material). Coussens et al. (2017) obtained five $^{40}\text{Ar}/^{39}\text{Ar}$ ages
213 from Centre Hills deposits (~0.79–0.48 Ma; Figure 1a; Table 1) and one from a fault block
214 within the Centre Hills (~1.31 Ma), which they interpret as originating from the Silver Hills
215 volcanic center. These ages were obtained from plagioclase phenocrysts, so the presence of
216 xenocrysts cannot be ruled out.

217 The questionable quality of the Silver Hills ages reported by Harford et al. (2002), and the
218 limited spatial and stratigraphic extent of the Silver Hills ages reported in Brown and Davidson
219 (2008) mean that the timing of volcanic activity is poorly known for the Silver Hills. This
220 highlights the need for new $^{40}\text{Ar}/^{39}\text{Ar}$ dates, to better constrain the timing of Silver Hills activity,
221 and aid the development of a detailed stratigraphy of the Silver Hills deposits.

222 **4.2. New $^{40}\text{Ar}/^{39}\text{Ar}$ Dates**

223 Here we present fifteen new $^{40}\text{Ar}/^{39}\text{Ar}$ ages for Montserrat (Figures 3–4; Table 2; supporting
224 information Tables S2–3): geographically eleven are from the Silver Hills (~2.17–0.45 Ma;
225 Figure 2) and four are from the Centre Hills (~1.04–0.38 Ma; Figure 1a). All samples produced
226 plateau ages that match our strict criteria. The first run of sample 17/76-AL did not yield a
227 plateau, however, and therefore did not meet the criteria for a reliable age, whereas the second
228 run yielded a release profile that meets our criteria and yielded an age of 1.18 ± 0.30 Ma.
229 Nevertheless, this age is viewed with caution as overall the sample shows significant
230 heterogeneity and non-reproducible release spectra (Figure 3).

231 Harford et al. (2002) note evidence for xenocrysts in their ages obtained from plagioclase
232 phenocrysts, leading them to interpret these ages as maximum ages, rather than true eruption
233 ages. The influence of xenocrysts in our sample ages can be assessed by examining the data
234 from samples 05/03-AL and 15/70-AC, for which both groundmass and plagioclase ages were
235 measured. For both samples the plagioclase age is systematically older than the groundmass age,
236 suggesting that the plagioclase may contain a minor xenocrystic component, but there is overlap
237 in the 2σ errors of the two phases, which suggests that the plagioclase ages encompass the true
238 eruption age within their 2σ errors. The plagioclase ages obtained by Coussens et al. (2017) also
239 likely represent the eruption ages, because they were obtained on similar material, and have
240 similar scale 2σ errors.

241 In the following sections, only the dates that are considered to be reliable are used in developing
242 a detailed stratigraphy of the Silver Hills deposits, and when discussing the timing of volcanic
243 activity.

244 **5. Lithofacies of the Silver Hills Deposits**

245 Here we adopt the non-genetic terminology of volcanic rocks proposed by White and Houghton
246 (2006); lithofacies terms and abbreviations used are given in Table 3. For debris avalanche
247 deposits we use the terms “megablock facies” (Voight et al., 2002) and “matrix facies” (Crandell
248 et al., 1984; Voight et al., 2002).

249 **5.1. Lava and Intensely Hydrothermally Altered Lava**

250 The lava exposures are dominantly composed of plagioclase-pyroxene-phyric andesite (~30–60
251 vol. % phenocrysts), with minor dacite and basaltic andesite with the same phenocryst
252 populations. Lava thickness ranges from meters to hundreds of meters, with some exposures
253 showing alignment of elongate crystals. The lava commonly locally transitions to breccia.
254 In some regions the lava flows are extensively hydrothermally altered to an extent that no
255 primary magmatic minerals are identifiable, and they exhibit a crumbly texture. The present day
256 exposures may be white or orange and yellow in color, with the latter being associated with
257 abundant centimeter-scale gypsum crystals. These altered exposures are surrounded by a halo of
258 less hydrothermally altered rocks, with the degree of hydrothermal alteration decreasing
259 outward.

260 **5.1.1. Interpretation**

261 The lavas form lava flows and domes, and the transitioning to breccia is interpreted as resulting
262 from local autobrecciation of the lava along its margins. The zones of intensely hydrothermally
263 altered lava are interpreted as the sites of fumarolic activity on the Silver Hills. The presence of
264 gypsum crystals and pervasive variable discoloration make them comparable to the recent
265 deposits of Galway’s Soufrière (Voight et al., 2002), which also shows the intensity of
266 hydrothermal alteration decreasing with distance from the fumaroles.

267 **5.2. Massive to Diffusely Stratified, Lapilli-Tuff to Tuff-Breccia (m-dsLT-TBr)**

268 The m-dsLT-TBr are poorly sorted, variably clast- and matrix-supported and consist of
269 centimeter- to meter-scale sub-rounded to angular andesite clasts, up to 20% of which are
270 hydrothermally altered. Some units of this facies display normal and inverse grading at their
271 upper and lower boundaries, respectively.

272 **5.2.1. Interpretation**

273 This facies is interpreted as block-and-ash flow deposits due to its massive structure, poor
274 sorting, clast size range and grading. These characteristics are comparable to the block-and-ash
275 flow deposits produced by dome collapses at Soufrière Hills Volcano during the 1995–2010
276 eruption (Cole et al., 2002; Stinton et al., 2014).

277 **5.3. Massive Tuff-Breccia and Breccia, with Megablocks (mTBr-Br_{MB})**

278 This facies is similar in appearance to the m-dsLT-TBr facies, but with three key differences:
279 absence of grading, presence of jigsaw-fit fractures in some clasts, and the occurrence of
280 megablocks. The megablocks are tens to hundreds of meters in scale, and can be split into two
281 categories: lava megablocks and volcanoclastic megablocks. Lava megablocks vary from poorly-
282 to highly-fractured and show variable hydrothermal alteration. Some of the megablocks are
283 faulted. Volcanoclastic megablocks are blocks of other volcanoclastic facies (e.g. mLT) hosted
284 within surrounding mTBr, and are either composed of a single unit or a layered sequence. Some
285 megablocks are sheared, and others contain parts which appear to intrude into the surrounding
286 breccia. Interdigitation of units within layered volcanoclastic megablocks is common. Most
287 boundaries between megablocks and breccia are sharp, but some display signs of mixing.

288 **5.3.1. Interpretation**

289 The presence of megablocks within the mTBr suggests that they are parts of debris avalanche
290 deposits; the megablocks are large coherent fragments of the original volcanic edifice that have
291 been transported by debris avalanches with little internal deformation. Layered volcanoclastic
292 megablocks may preserve their original structure and stratigraphy. The matrix facies consists of a
293 poorly-sorted massive breccia formed from the mingling of disaggregated megablocks and
294 entrained material. Jigsaw-fit fracturing of clasts is a common feature of debris avalanche
295 deposits (e.g. Crandell et al., 1984; Ui, 1983; Ui & Glicken, 1986), as are the fluidal textures at
296 the edges of megablocks and deformation of units within individual volcanoclastic megablocks
297 (e.g. interdigitation of units) (e.g. Takarada et al., 1999; Ui & Glicken, 1986; van Wyk de Vries
298 & Davies, 2015). Faulting is another well-documented feature of some megablocks (e.g.
299 Glicken, 1996; Ui et al., 1986; Ui & Glicken, 1986; van Wyk de Vries & Davies, 2015).

300 **5.4. Massive Lapilli-Tuff, with regular Lapilli-Tuff and Tuff-Breccia Lenses** 301 **(mLTlensLT-TBr)**

302 The mLT are poorly-sorted, matrix-supported and consist of centimeter-scale rounded to sub-
303 rounded andesite clasts, ~10% of which are hydrothermally altered. The LT-TBr lenses are
304 poorly sorted, clast supported and consist of centimeter- to decimeter-scale rounded andesite
305 clasts, up to 5% of which are hydrothermally altered. They typically have meter- and decimeter-
306 scale length and thickness, respectively, with decimeter-scale spacing.

307 **5.4.1. Interpretation**

308 This facies is interpreted as lahar deposits, on the basis that they contain multiple coarse lenses
309 of rounded to sub-rounded andesite clasts in variably massive and parallel to cross-stratified
310 coarse ash to coarse lapilli. They are similar to modern lahar deposits present in the Belham
311 Valley, on the west flank of Soufrière Hills (Barclay et al., 2007).

312 **5.5. Pumiceous, Massive to Diffusely Stratified, Lapilli-Tuff to Tuff-Breccia (pm-dsLT-**
313 **TBr)**

314 This facies can be split into two subfacies: well-sorted and poorly-sorted. Occurrences of the
315 well-sorted subfacies are clast-supported with centimeter-scale sub-angular to angular clasts of
316 andesitic pumice and andesite. Clast proportions are typically ~90% pumice and ~10% andesite,
317 with the pumice clasts being consistently coarser than the andesite clasts. Exposures of the
318 poorly-sorted subfacies are variably clast- and matrix-supported and consist of centimeter- to
319 decimeter-scale rounded to angular clasts. The clast proportions are typically in the range of 65–
320 99% pumice, 1–33% andesite and 0–5% HA andesite. Locally, exposures of this subfacies have
321 erosional bases.

322 **5.5.1. Interpretation**

323 The well-sorted subfacies are interpreted as primary fallout deposits, due to the high degree of
324 sorting and predominance of angular pumice with subordinate smaller lithics. The poorly-sorted
325 subfacies are interpreted as pumice-and-ash flow deposits, due to their poor sorting, rounded
326 clasts and erosional bases, similar to pumice-and-ash flow deposits produced from recent
327 Vulcanian eruptions of Soufrière Hills (Cole et al., 2002, 2014).

328 **6. Stratigraphy of the Silver Hills**

329 **6.1. Little Bay to South Drummonds, >2 Ma**

330 The oldest dated unit is an isolated exposure of dacitic mLT-TBr at south Drummonds. This unit
331 contains meter-scale blocks, has a minimum thickness of 3 m, and is dated at 2.170 ± 0.180 Ma
332 (Figure 2).

333 **6.2. Marguerita Ghaut and North Marguerita Bay, ~1.7–1.6 Ma**

334 Marguerita Ghaut contains mTBr and coherent andesite and basaltic andesite lava exposures,
335 with sharp boundaries between them. The mTBr has an age of 1.682 ± 0.094 Ma (Figure 2).
336 The eastern mouth of the ghaut contains a ~35 m thick sequence of mTBr, and an andesite block
337 from the base of this sequence has an age of 1.634 ± 0.083 Ma (Figure. 2). North Marguerita Bay
338 contains a debris avalanche deposit consisting of a volcanoclastic megablock overlain by a
339 mTBr_{MB} (Figure 5; see supporting information Text S1 for a detailed description).

340 **6.3. Yellow Hole to Old Quaw, ~1.5 Ma**

341 The Yellow Hole exposures consist of extensively hydrothermally altered andesite lava overlain
342 by non-altered lava dated at 1.520 ± 0.051 Ma (Brown & Davidson, 2008). At the mouth of Old
343 Quaw ghaut is a debris avalanche deposit (Figure 2), with a megablock of hydrothermally altered
344 lava next to non-altered mBr (matrix facies), and the boundary between them varies from sharp
345 to transitional. There is an isolated block of the breccia within the hydrothermally altered lava,
346 most likely resulting from internal deformation during transport (Siebert, 1984).

347 **6.4. North West Bluff, ~1.5–4 Ma**

348 North West Bluff is a ~200 m high peak made of andesite lava with areas of local (<1 m²)
349 hydrothermal alteration, and an age of 1.493 ± 0.098 Ma. Exposure of this lava continues as a
350 ridge heading southeast from North West Bluff to Valentine Hill (Figure 2), which consists of
351 hydrothermally altered lava overlain by non-altered lava. In northwest Thatch Valley, the lavas
352 have undergone extensive hydrothermal alteration, and locally becomes the ‘intensely
353 hydrothermally altered lava’ facies.

354 North-central Thatch Valley contains a ~45 m thick (minimum) mTBr which has an age of 1.450
355 ± 0.160 Ma (Figure 2). Some clasts contain jigsaw-fit fractures, which supports an origin as a

356 debris avalanche deposit, but the limited size of the exposure, coupled with the buried boundaries
357 with surrounding units makes this difficult to confirm.

358 The andesite and dacite lava around and north of Rendezvous Bay is of a similar age, $1.424 \pm$
359 0.080 Ma (Figure 2). There is exposure of ‘intensely hydrothermally altered lava’ midway
360 between Rendezvous Bay and North West Bluff.

361 **6.5. Silver Hill, ~1.4 Ma**

362 Andesite lavas and mLT-Br’s tens of meters thick are exposed alongside the road between
363 Drummonds and Silver Hill, and have been dated at 1.430 ± 0.019 to 1.395 ± 0.017 Ma (Brown
364 & Davidson, 2008) (Figure 2). Rendezvous Bluff consists of a ~50 m high sequence of m-dsTBr
365 overlying the lavas of Rendezvous Bay. Near Rendezvous they have a flow direction away from
366 Silver Hill (Figure 2), and so are likely contemporaneous with the block-and-ash flow deposits
367 between Silver Hill and Drummonds.

368 Further block-and-ash flow deposits from this period can be found overlying the basal
369 hydrothermally altered lava of Valentine Hill (Figure 2). A ridge of this lava extends southeast
370 from Valentine Hill, and on the southwestern side of this ridge the lava is overlain by a ~20 m of
371 m-dsTBr’s (units V1–4) infilling a palaeovalley (Figure S1).

372 The lavas of Thatch Valley are locally overlain by mTBr, which locally has a hydrothermally
373 altered matrix. These breccias are likely contemporaneous with the other mTBr units.

374 **6.6. South Marguerita Bay, ~1.3 Ma**

375 South Marguerita Bay contains a sequence of dacitic mLT-TBr tens of meters thick. The upper
376 unit of this sequence is dated at 1.330 ± 0.190 Ma (Figure 2). Coussens et al. (2017) obtained an
377 age of 1.310 ± 0.200 for their ‘South Lime Kiln Bay pumice’ unit, which is a poorly-sorted

378 pmLT located in a fault block within the Centre Hills (Figure 1a). Due to its age, and location in
379 a fault block, they interpret this deposit as originating from the Silver Hills.

380 **6.7. Little Bay, ~1.0–0.8 Ma**

381 The largest debris avalanche deposit of the Silver Hills is located in the Little Bay region,
382 spanning Potato Hill, Davy Hill and Little Bay (Figure 2, S2 and S3). It consists of lava- and
383 volcanoclastic-megablocks, with surrounding matrix facies (see supporting information Text S2
384 for a detailed description). Lava from a megablock east of Potato Hill has an age of $1.430 \pm$
385 0.120 Ma.

386 **6.8. Potato Hill, ~0.8 Ma**

387 Overlying unit PH1 at Potato Hill is a pumiceous pyroclastic sequence (units PH2–4; Figure 2
388 and 6a). Unit PH3 (primary fallout deposit) has been dated at 0.800 ± 0.120 Ma (Figure 2), and
389 has a Centre Hills origin (see section 8.1). This constrains the timing of the Little Bay debris
390 avalanche to >0.8 Ma.

391 **6.9. Old Quaw Ghaut, ~0.45 Ma**

392 The Old Quaw debris avalanche deposit is overlain by a horizontally bedded volcanoclastic
393 sequence containing four units, three of which are separated by palaeosols (units OQ1–4; Figure
394 6b), and were likely deposited in a palaeovalley. The base of this sequence, a $mLT_{lensLT-TBr}$ (unit
395 OQ1), is overlain by pumiceous deposits which display noticeable variation between two
396 exposures ~60 m apart (log sites 2–3; Figures 2 and 6b). Units OQ2a and 3a laterally transition
397 between the well- and poorly-sorted subfacies' of pmLT-TBr with small (centimeter-scale)
398 erosional channels. At log site 2 they grade into coarser and finer grained poorly-sorted pmLT-
399 TBr's, respectively, with higher proportions of lithic clasts and matrix. This grading of unit

400 OQ2a is also displayed at log site 3, but here unit OQ3a is missing. Unit OQ2a has been dated at
401 0.450 ± 0.130 Ma. The transition between the well- and poorly-sorted subfacies within the same
402 unit suggests that units OQ2–3 are reworked fallout deposits. This interpretation is supported by
403 the $^{40}\text{Ar}/^{39}\text{Ar}$ age and Pb isotope data, because the pumice clasts from unit OQ2a have a
404 Soufrière Hills signature (see section 8.1). It is considered unfeasible for a pyroclastic density
405 current to reach the eastern Silver Hills from the Soufrière Hills, hence these pumice clasts are
406 likely to be derived from fallout from an eruption column. This unit is the oldest known deposit
407 from a Soufrière Hills eruption.

408 **7. Expanded Stratigraphy of the Centre Hills**

409 **7.1. East Coast, ~1 Ma**

410 Sample 21/81-AC comes from a basaltic andesite mTBr on the east coast of Centre Hills (Figure
411 1a), which lies at the base of the stratigraphy of Coussens et al. (2017). The age of 1.040 ± 0.250
412 Ma is within error of the oldest dates for this center (Coussens et al., 2017; Harford et al., 2002).

413 **7.2. Southwest Centre Hills, ~0.45 Ma**

414 Pumice from a pumiceous mTBr in the southwest Centre Hills has an $^{40}\text{Ar}/^{39}\text{Ar}$ age of 450 ± 170
415 ka (Figure 1a), and a Soufrière Hills Pb isotope signature (see section 8.1). This provides further
416 evidence for Soufrière Hills volcanism at ~450 ka.

417 **7.3. Dry Waterfall and Spring Ghaut, ~0.38 Ma**

418 Andesite lava from Dry Waterfall (central Centre Hills) has been dated at 378 ± 18 ka (Figure
419 1a), and has a Centre Hills Pb isotope value (section 8.1), providing the youngest known age for
420 Centre Hills volcanism. A dacitic mTBr from Spring Ghaut (southwest Centre Hills) has been

421 dated at 376 ± 85 ka (Figure 1a), and has a Soufrière Hills Pb isotope signature. This
422 demonstrates an overlap in activity between Centre Hills and Soufrière Hills volcanism.

423 **8. Provenance**

424 Many intra-oceanic arcs display along-arc geochemical heterogeneity, caused by variations in
425 source component contributions (e.g. Izu-Bonin-Mariana arc: Elliott et al. (1997); Ishizuka et al.
426 (2007); Tonga-Kermadec-Lau arc: Ewart et al. (1998); Lesser Antilles arc: Macdonald et al.
427 (2000)). Such variation has also been observed on individual islands, allowing the eruption
428 deposits of distinct volcanic centers on an island to be distinguished using isotope and trace
429 element ratios. For example, Pagan island in the Marian arc contains two volcanic centers ~8 km
430 apart, Mount Pagan and South Pagan, whose eruption deposits can be distinguished using trace
431 element ratios (e.g. Ba/Th, Ba/La, Nb/Zr) (Marske et al., 2011). The island of Hachijojima in the
432 Izu-Bonin arc comprises two volcanic centers ~7 km apart, Higashiyama and Nishiyama, the
433 eruption deposits of which can be distinguished using Pb isotopes, and Zr/Y and La/Sm ratios
434 (Ishizuka et al., 2008). In the Lesser Antilles, there is a clear north-south gradient in the Sr, Nd
435 and Pb isotope ratios, and trace element patterns of volcanic rocks along the entire arc that has
436 been present for ~5 Myr (Labanieh et al., 2010; Lindsay et al., 2005). This geographical pattern
437 is also observed on individual islands, such as Martinique, where $^{143}\text{Nd}/^{144}\text{Nd}$ can be used to
438 separate deposits from Pitons du Carbet and Mont Conil-Mont Pelée, which overlapped in
439 activity 545–322 ka (Germa et al., 2011b; Labanieh et al., 2012). For Montserrat, Pb isotopes
440 have been shown to clearly distinguish Soufrière Hills deposits from those of the Centre and
441 Silver Hills, and $^{143}\text{Nd}/^{144}\text{Nd}$ can be used to differentiate between Silver Hills and Centre Hills
442 deposits (Cassidy et al., 2012).

443 For some samples in this study there is ambiguity over which volcanic center they are from, such
444 as 16/72-PR which is geographically within the Silver Hills, but has a Centre/Soufrière Hills age.
445 Here, we use trace element and isotope geochemistry to help constrain their provenance (data is
446 presented in supporting information Table S4).

447 **8.1. Terrestrial Deposits**

448 Most of the samples analyzed in this paper fit within the Silver Hills-Centre Hills Pb isotope
449 field, with three samples falling in the Soufrière Hills field: 28/57-AC, 16/72-PR and 20/79-PC
450 (Figure 7).

451 Silver Hills and Centre Hills samples can be distinguished on a plot of $^{143}\text{Nd}/^{144}\text{Nd}$ vs Nb/Y
452 (Figure 8). Four samples with uncertain origin (i.e. from either Silver Hills or Centre Hills
453 volcanism) are highlighted on Figure 8a: pumice from Davy Hill, Potato Hill and Lime Kiln Bay,
454 and a lava clast from South Marguerita Bay. Pumice from a fault block in South Lime Kiln Bay
455 (sample 11.1.4C), which is geographically part of the Centre Hills, has been dated at ~1.31 Ma,
456 leading to the interpretation that this deposit originated from Silver Hills volcanism (Coussens et
457 al., 2017). This interpretation is supported by $^{143}\text{Nd}/^{144}\text{Nd}$ vs Nb/Y, in which this same sample
458 plots within the Silver Hills field (Figure 8a).

459 The Silver Hills-Centre Hills boundary defined by Harford et al. (2002) follows Brimm's Ghaut,
460 which runs through Marguerita Bay (Figure 2). Sample 12/13-AC from south Marguerita Bay
461 (south of the boundary) has been dated at ~1.33 Ma, suggesting a Silver Hills origin. This is
462 supported by $^{143}\text{Nd}/^{144}\text{Nd}$ vs Nb/Y (Figure 8a), suggesting that the boundary between the Silver
463 Hills and Centre Hills is further south than previously thought.

464 Sample 23/86-PF (unit PH3 on Potato Hill) is geographically within the Silver Hills, but has an
465 age of ~0.8 Ma, suggesting this deposit is derived from the Centre Hills (Figure 2). This
466 interpretation is supported by a Centre Hills geochemical signature (Figure 8a). The pumice
467 sample from Davy Hill (24/88-PC) is also geographically within the Silver Hills, but falls in the
468 Centre Hills field in Figure 8a, suggesting a Centre Hills origin. Because this sample is part of
469 the Little Bay debris avalanche deposit, this suggests that the debris avalanche occurred during
470 the early stages of Centre Hills volcanism.

471 **8.2. Marine Tephra Deposits**

472 Marine sediment core U1396C contains fifteen tephra layers with thicknesses >1 cm within the
473 ~2.35–0.37 Ma time span covered by our new $^{40}\text{Ar}/^{39}\text{Ar}$ ages. The age assignments of the tephra
474 layers are derived from palaeomagnetic, biostratigraphic and foraminifera $\delta^{18}\text{O}$ correlations
475 (Fraass et al., 2016; Hatfield, 2015). Pb isotope analyses show that thirteen of these layers are
476 from Montserrat and the other two are from Guadeloupe (Palmer et al., 2016). Of the Montserrat
477 layers, eight contain enough pumice or fresh non-vesicular lava grains for geochemical analysis
478 (Table 4). Of particular interest are the five tephra layers in the 1–1.3 Ma period (the gap in the
479 terrestrial age record between the Silver and Centre Hills) with sufficient pumice. Figure 8b
480 shows that the layers with ages of 1.10 Ma and 1.03 Ma fall within the Silver Hills field, and
481 1.14, 1.08 and 1.04 Ma fall within the Centre Hills field (Figure 8b). The absolute uncertainty in
482 the age of any individual tephra layer is ~50 kyr, but the stratigraphic order of the layers is
483 certain. Hence, we can be confident that there was overlap in activity between the Silver and
484 Centre Hills for at least ~130 ka.

485 **9. Petrology**

486 The lavas of the Silver Hills volcanic center are porphyritic (~30–60 vol. % phenocrysts) with a
487 phenocryst assemblage of ~65–75% plagioclase up to 4 mm, ~15–20% orthopyroxene up to 6
488 mm and ~5–15% clinopyroxene up to 5 mm. Quartz and amphibole are locally present in minor
489 amounts. Zoning is observed in some clinopyroxene and orthopyroxene phenocrysts, and all
490 plagioclase phenocrysts, with many of the latter displaying sieve textures. The groundmass is
491 generally microcrystalline and composed of plagioclase, orthopyroxene, clinopyroxene and Fe-
492 Ti oxides (Figure 9), with some samples showing alignment of elongate crystals.

493 Enclaves are abundant within Silver Hills lavas, and comprise up to 20 vol. %. They have
494 coarser groundmasses (composed of plagioclase, orthopyroxene, clinopyroxene and Fe-Ti
495 oxides) than the host andesite, with a higher proportion of pyroxenes (Figure 9). Many of the
496 enclaves have a diktytaxitic groundmass, with interlocking, randomly-orientated elongate
497 crystals, similar to enclaves erupted during the 1995–2010 eruption of the Soufrière Hills (Plail
498 et al., 2014).

499 The Centre Hills samples have a similar phenocryst assemblage as the Silver Hills lavas, closely
500 matching the samples described by Coussens et al. (2017). The Soufrière Hills samples are
501 porphyritic (~30 vol. % phenocrysts) with a phenocryst assemblage of ~65–75% plagioclase, 15–
502 20% orthopyroxene and 10–15% amphibole, with minor clinopyroxene and quartz, similar to the
503 Soufrière Hills lavas erupted in the past ~130 kyr (Harford et al., 2002).

504 **10. Discussion**

505 **10.1. Evolution of the Silver Hills Volcanic Center**

506 Subaerial volcanic activity began in the Silver Hills prior to 2 Ma, with the oldest rocks present
507 as lava domes around the Little Bay area and dome collapse deposits built up the south

508 Drummonds region (Figure 10). At ~1.7–1.6 Ma, activity migrated to the eastern part of Silver
509 Hills, forming the lava domes and associated deposits of Marguerita Bay. Part of this edifice
510 collapsed to form the Marguerita Bay debris avalanche deposit. Activity continued in this region
511 up until ~1.5 Ma, forming the lavas of Yellow Hole, with collapse of this edifice forming the Old
512 Quaw debris avalanche. Next, activity shifted to the northwestern part of the Silver Hills,
513 forming the lava domes of North West Bluff, Thatch Valley and Rendezvous Bay at ~1.5–1.4
514 Ma, with concomitant hydrothermal activity producing the observed fumarole deposits in this
515 region. At ~1.4 Ma activity shifted again to form lava domes at Silver Hill and Drummonds,
516 which collapsed to form block-and-ash flow deposits throughout the north, west and center of the
517 Silver Hills. Collapse of these edifices with part of the young Centre Hills edifice created the
518 Little Bay debris avalanche deposit at around ~1–0.8 Ma. The block-and-ash flow deposits of
519 south Marguerita Bay suggest that lava dome growth was still active in the Drummonds area
520 ~1.35–1.30 Ma (Figure 10). The youngest deposits found in the Silver Hills region are reworked
521 pumice fall deposits in Old Quaw, which Pb isotopes indicate to be derived from eruptions of the
522 early stages of Soufrière Hills volcanism ~0.45 Ma.

523 **10.2. Comparisons with Soufrière Hills and Centre Hills**

524 The Silver Hills is the smallest volcanic center on Montserrat in terms of subaerial exposure, but
525 bathymetric data may provide an insight into its original size. Montserrat is surrounded by a
526 shallow submarine shelf, which extends up to 5 km wide around the Silver Hills (Figure 1), and
527 is interpreted as representing the original expanse of the Silver Hills (Le Friant et al., 2004).
528 Assuming that the Silver Hills originally had a similar size to the Soufrière Hills, the estimated
529 minimum original volume of the Silver Hills above 100 m below sea level (the depth of the

530 submarine shelf) is 17 km³; the subaerial part of the Soufrière Hills is ~12 km³ (Le Friant et al.,
531 2004).

532 Our work on the deposits of the Silver Hills volcano has shown its past volcanic activity to be
533 similar to that of the Soufrière Hills, with both characterized by lava dome growth and collapse
534 coupled with Vulcanian eruptions and periodic flank/sector collapses. Soufrière Hills does,
535 however, exhibit evidence of larger, sustained eruptions at ~450 and ~179 ka, whereas there is
536 no record of large eruptions emanating from the Silver Hills. The Centre Hills activity is also
537 characterized by lava dome growth and collapse with Vulcanian eruptions, but also produced
538 multiple Plinian eruptions (possibly up to magnitude 5) throughout its eruptive history (Coussens
539 et al., 2017; Harford et al., 2002). The consistency in the style of volcanic activity throughout
540 the lifespan of the Silver Hills adds support to the hypothesis of Harford et al. (2002) that future
541 activity at Soufrière Hills is likely to continue in the same style as the 1995–2010 eruption.

542 It is worth noting, however, that the exposed massifs of the Soufrière Hills and Centre Hills are
543 both currently larger in size than Silver Hills, and that the Plinian deposits of both the former are
544 situated along coastal exposures that are now missing from Silver Hills. Additionally, the
545 current size of the sub-aerial portion of Silver Hills is approximately the same size as the central
546 dome complex of the Soufrière Hills which, like the central part of Centre Hills, is dominated by
547 massive andesite dome-lava and their collapse deposits (Harford et al., 2002). Thus it is feasible
548 that any large sustained explosive eruptions that Silver Hills may have produced are not
549 preserved on land, akin to the Basal Complex, the oldest volcanic center on Basse-Terre,
550 Guadeloupe. This is another deeply eroded volcano whose sub-aerial record is dominated by
551 effusive eruption products, with no evidence of large explosive activity. However, the study of a
552 marine sediment core has revealed that this seemingly effusive center produced a large Plinian

553 eruption (Volcanic Explosivity Index ~6) towards the end of its life, at ~2.4 Ma, which is
554 believed to be the largest known eruption in the Lesser Antilles (Palmer et al., 2016). While the
555 Silver Hills may not have produced eruptions of this magnitude, this example serves to highlight
556 a potential preservation bias within the Silver Hills' terrestrial record.

557 **10.3. Comparisons with Other Arc Volcanic Centers**

558 Many arc volcanoes that are dominated by andesitic and dacitic lava dome formation
559 nevertheless also experience periodic Plinian eruptions, similar to the Centre Hills. For example,
560 the 1902 Plinian eruption of Santa Maria, a dominantly andesitic (Rose, 1972) stratovolcano in
561 Guatemala, was one of the 10 largest eruptions ever observed (Bennett et al., 1992), yet volcanic
562 activity at Santa Maria has been dominated by eruptions of lava flows and domes, with their
563 associated collapse pyroclastic deposits (Rose, 1972, 1973, 1987). Indeed, the active Santiaguito
564 dome complex has built up inside the crater produced from the 1902 eruption. In Chile, Volcán
565 Quizapu produced two of the largest historical eruptions of South America, which were of a
566 similar composition, yet one was effusive (a ~5 km³ mingled andesite-dacite lava flow in 1846–
567 1847), and one was explosive (a ~4.5 km³ dacitic Plinian eruption in 1932) (Hildreth & Drake,
568 1992). The transition between effusive and explosive eruptions at Volcán Quizapu has been
569 linked to the extent of mafic magma recharge and mixing prior to eruption. The 1932 Plinian
570 eruption had a relatively minor recharge component, while the recharge magma comprised <10–
571 45 vol% of the lava erupted throughout 1846–1847 (Ruprecht & Bachmann, 2010). The resident
572 magma temperatures for both eruptions is estimated to be ~870°C (Ridolfi et al., 2010), but the
573 greater volume of recharge magma of the 1846–1847 eruption led to an eruption temperature up
574 to 130°C hotter than the 1932 eruption. This higher magmatic temperature enhanced syneruptive

575 magma degassing and led to effusive eruptive behavior, by accelerating volatile diffusion,
576 lowering melt viscosity, and inhibiting brittle fragmentation (Ruprecht & Bachmann, 2010).

577 Magma recharge and mixing is also considered to be responsible for the long-term (~500–0 ka)
578 low explosivity of Mount Hood, Oregon, another andesite-dacite arc volcano with no evidence
579 for large explosive eruptions (Koleszar et al., 2012; Scott et al., 1997). Viscosity models show
580 that mafic recharge beneath Mount Hood may result in a 5–10-fold decrease in viscosity of the
581 silicic resident magma, facilitating greater diffusion of volatiles, and delaying or preventing
582 fragmentation during magma ascent. The continued low explosivity of activity at Mount Hood
583 over 500 kyr is thought to be due to somewhat constant mixing proportions and timescales,
584 whereas variability in mixing proportions and timescales leads to variation in eruption styles
585 between effusive and explosive (Koleszar et al., 2012), such as observed at Volcán Quizapu
586 (Ruprecht & Bachmann, 2010). Further, Koleszar et al. (2012) invoke this model to explain the
587 long-term low explosivity (i.e. absence of Plinian eruptions) in other andesitic-dacitic arc
588 volcanoes where magma mixing is a common process, such as Unzen volcano, Japan
589 (Hoshizumi et al., 1999; Venezky & Rutherford, 1999), and Mount Dutton, Alaska (Miller et al.,
590 1999).

591 On Montserrat, this model may also explain the low explosivity behavior of the Silver Hills and
592 Soufrière Hills, because the lavas of these centers contain abundant mafic enclaves, indicating
593 magma mixing has consistently played a major role in controlling eruption styles at these
594 volcanic centers (e.g. Murphy et al., 1998; this study). Furthermore, for the Centre Hills
595 deposits, enclaves are only present within lavas, and not in the pumiceous (explosive) deposits
596 (Coussens et al., 2017). This suggests that the absence of, or at least reduced extent of, magma
597 recharge and mixing may have played a significant role in producing large explosive eruptions at

598 the Centre Hills. However, this model relies on the recharge magma raising the temperature of
599 the resident magma to prevent explosive eruptions, but geothermometry studies estimate that
600 magma storage temperatures beneath the Centre Hills (~810–1080°C; Coussens et al., 2017)
601 were similar to those of the 1995–2010 Soufrière Hills eruption (~785–1100°C; Barclay et al.,
602 1998; Christopher et al., 2014; Devine et al., 1998, 2003, Murphy et al., 1998, 2000). This
603 suggests that the rise in temperature, and its associated effects, cannot alone be responsible for
604 the explosive eruptions of the Centre Hills. Coussens et al. (2017) showed that the composition
605 of Center Hills deposits remained constant, thus ruling out changes in magma composition as
606 influencing eruption styles. They suggest instead that explosive eruptions may have been the
607 result of local changes in magma storage conditions (altering magma temperature or viscosity)
608 and pre-eruptive dynamics.

609 In the Lesser Antilles, Silver Hills volcanism is typical of that documented along the northern
610 arc, in that andesitic dome growth and collapse—with small explosive eruptions—has dominated
611 volcanic activity at Saba, St. Eustatius, St. Kitts, and Nevis, with no evidence for larger,
612 sustained eruptions (Baker, 1984, 1985; Baker et al., 1980; Davidson & Wilson, 2011; Defant et
613 al., 2001). Petrological evidence (e.g. reverse-zoned phenocrysts) indicate that magma recharge
614 and mixing is a common process at Saba and St. Kitts (Baker et al., 1980; Toothill et al., 2007),
615 which following the model of Koleszar et al. (2012), suggests that the characteristics of magma
616 recharge and mixing have been constant for the northern islands, thus inhibiting the potential for
617 large explosive eruptions and maintaining low explosivity behavior. The central and southern
618 islands display similar activity to the northern islands, but with Plinian eruptions identified at La
619 Soufrière, Guadeloupe (Komorowski et al., 2005), Morne Diablotins and Morne Trois Pitons-
620 Microtrin, Dominica (Boudon et al., 2017), Mont Pelée, Martinique (Roobol & Smith, 1976;

621 Westercamp & Traineau, 1983), Qualibou, St Lucia (Wohletz et al., 1986), and Soufrière, St
622 Vincent (Rowley, 1978; Wright et al., 1984), more akin to the Centre Hills volcanism (Coussens
623 et al., 2017). In Dominica, mafic enclaves are present in lavas from multiple volcanic centers,
624 but are notably absent from pumiceous deposits (Howe et al., 2015), further supporting a link
625 between magma recharge and mixing and eruption explosivity. Further detailed studies
626 comparing evidence for magma mixing (e.g. enclave abundances, reverse-zoned phenocrysts) in
627 lava samples with Plinian pumice samples from multiple volcanic centers would provide a more
628 thorough assessment of the link between magma mixing and eruption explosivity in the Lesser
629 Antilles.

630 **10.4. Revised Geochronology of Volcanism on Montserrat**

631 Here, we present a revised geochronology of volcanic activity of Montserrat's three main
632 volcanic centers (Figure 11), based on a review of existing ages, new $^{40}\text{Ar}/^{39}\text{Ar}$ dates, and
633 palaeomagnetic ages from marine tephra layers.

634 Previously, Silver Hills volcanism was dated to range from ~2.6–1.2 Ma (Brown & Davidson,
635 2008; Harford et al., 2002), but as discussed some of these dates are unreliable. Silver Hill
636 volcanism can now be reliably constrained to at least ~2.17–1.03 Ma. Coussens et al. (2017)
637 divided Centre Hills volcanism into two periods of activity, spanning >0.95 to ~0.60 Ma and
638 ~0.60 to ~0.40 Ma. The new Centre Hills dates presented in this study expand the timing of
639 Centre Hills volcanism by ~0.2 Myr, to ~1.14–0.38 Ma.

640 Three stages of Soufrière Hills volcanism have been previously recognized: >300–175 ka, 175–
641 130 ka and 112 ka to recent (Coussens et al., 2017; Harford et al., 2002). Our new ages identify
642 a fourth, earlier stage, ~450–300 ka, characterized by the eruption of hornblende-orthopyroxene
643 andesites, similar to lavas erupted since ~112 ka, and in contrast to the two-pyroxene andesites

644 erupted ~290–130 ka (Harford et al., 2002; Rea, 1974). This means that the petrology of the
645 Soufrière Hills eruptive products has changed at least twice throughout the volcano's
646 development. Garibaldi Hill, which contains a two-pyroxene andesite block-and-ash flow
647 deposit dated at 290 ka (Harford et al., 2002), contains both two-pyroxene and hornblende-
648 hypersthene andesites, but the stratigraphic relationship between the two andesite types is not
649 documented (Rea, 1974). A detailed stratigraphy of Garibaldi Hill may provide further details as
650 to when the change from hornblende-hypersthene to two-pyroxene andesite took place, and if it
651 was an instant or a gradual change.

652 Our new ages show that Silver, Centre and Soufriere Hills were active for at least 1.14 Myr, 0.76
653 Myr, and 0.45 Myr, respectively. The most comparable island to Montserrat in the Lesser
654 Antilles arc is the neighboring island of Basse-Terre, Guadeloupe. It too was formed following
655 tectonic adjustments during the Mid-Miocene and it also shows a north-south migration in the
656 locus of volcanism over a similar time interval. There is also high quality age data available for
657 the volcanic centers on Basse-Terre; with 2.79–2.68 Ma, 1.81–1.15 Ma, 1.02–0.44 Ma, 0.56–
658 0.47 Ma and 0.21 Ma – present recorded for the Basal Complex, Septentrional Chain, Axial
659 Chain, Monts Caraïbes Massif and Grande Découverte Volcanic Complex, respectively (Carlut
660 et al., 2000; Ricci et al., 2015a, 2015b, Samper et al., 2007, 2009). With the exception of the
661 oldest Basal Complex (which is heavily eroded and has limited subaerial exposure) and Monts
662 Caraïbes Massif (which has limited subaerial exposure and only two dates), these intervals of
663 activity (0.66 Myr, 0.58 Myr, and 0.21 Myr) for the different centers on Basse-Terre are similar
664 to those observed on Montserrat. These observations suggest that ~0.5–1.0 Ma is a common
665 lifespan for volcanic centers in the region. The question arises, therefore, as to whether this
666 apparent timescale of volcanic center duration is purely stochastic or whether it has more

667 fundamental significance. For example, the duration of a volcanic center may be related to the
668 life cycle of volcanic edifices. Modelling of edifice loading indicates that progressive growth of
669 a volcanic structure results in the confining pressure increasing to the extent that the center is
670 forced to migrate laterally (Pinel et al., 2010). Alternatively, the duration of a volcanic center
671 may be related to deeper processes. For example, it has been suggested that partial melting in
672 the mantle wedge yields rising diapirs of partially molten material that rise through the mantle
673 with frequencies of order 10^5 – 10^6 years (Hall & Kincaid, 2001; Stern, 2002). Further detailed
674 geochronology of volcanic centers on other islands of the Lesser Antilles is required to assess
675 these hypotheses in more detail.

676 Our new ages also provide evidence for a ~130 kyr overlap in activity between the Silver and
677 Centre Hills, and ~70 kyr overlap between the Centre and Soufrière Hills. There was also
678 overlap between the Soufrière and South Soufrière Hills (Cassidy et al., 2012, 2014). Overlap in
679 volcanic activity between two or more centers on an individual island has also been documented
680 on Martinique, where Trois Ilets and Pitons du Carbet were both active from 998 to 345 ka.
681 Here, further coeval activity occurred at Mont Conil-Mont Pelée during 545–345 ka (Germa et
682 al., 2010, 2011b). On Dominica, there has been coeval activity between at least up to four
683 volcanic centers over much of the lifetime of the island (Smith et al., 2013, and references
684 therein). The volcanic centers of Basse-Terre, Guadeloupe have been extensively dated, and
685 overlap in activity has only been identified between two centers: the Axial Chain and Monts
686 Caraïbes during 555–472 ka (Carlut et al., 2000; Ricci et al., 2015a, 2015b, Samper et al., 2007,
687 2009).

688 The overlap in volcanic activity between centers on these four islands suggests that it is a
689 common phenomenon in the Lesser Antilles and, indeed, in other arc systems. For example, in

690 the Izu-Bonin-Mariana arc, most islands contain a single volcanic center, but islands with
691 multiple centers have experienced coeval activity at two neighboring volcanic centers. These are:
692 Hachijojima, where Higashiyama and Nishiyama (7 km apart) have been concurrently active for
693 at least 10 ka (Ishizuka et al., 2008); Pagan island, where Mount Pagan and South Pagan (~8 km
694 apart) have experienced coeval activity for at least 64 ka (Marske et al., 2011); and Izu-Oshima,
695 which has been simultaneously active with the neighboring Izu-Tobu volcanic field for at least
696 40–50 ka, which at their closest are only ~4 km apart (Ishizuka et al., 2015 and references
697 therein). The distance separating sites of coeval activity in the Izu-Bonin-Mariana and Lesser
698 Antilles arcs (typically <10 km) relative to the depth to the melt generation zone above the
699 subducting slab (of the order ~100 km; Stern, 2002) suggests that a rising diapir or plume of
700 partial melt may bifurcate to form separate magma chambers at intermediate depths (~15 km;
701 Odbert et al., 2014) beneath the individual volcanic centers.

702 **11. Conclusions**

703 We describe the rocks of the Silver Hills volcanic center, which are dominated by andesite lavas
704 and breccias, formed from effusive lava dome eruptions and dome collapses. Pumiceous flow
705 deposits are also present, providing evidence of explosive activity from Vulcanian style
706 eruptions. There is evidence of widespread hydrothermal alteration, with three fumarole deposits
707 identified, resulting from hydrothermal activity concurrent with Silver Hills volcanism. Four
708 debris avalanche deposits were also identified, indicating that the volcano experienced periodic
709 sector collapses. These observations suggest that the Silver Hills was characterized by the same
710 type of volcanic activity as has been observed at the Centre Hills and Soufrière Hills. The
711 notable absence of evidence of sustained explosive eruptions at Silver Hills, which occurred in
712 the early stages of Soufrière Hills' development and throughout Centre Hills' activity, may be the

713 result of consistent mafic magma recharge and mixing, which can raise magma temperatures and
714 inhibit the potential for large explosive eruptions.

715 New $^{40}\text{Ar}/^{39}\text{Ar}$ dates, combined with ages from marine tephra layers and a review of existing
716 ages, have yielded a revised geochronology of volcanic activity of Montserrat's three main
717 centers, which were active during at least ~2.17–1.03 Ma, ~1.14–0.38 Ma, and ~0.45 Ma–present
718 for the Silver, Centre, and Soufrière Hills centers, respectively. Two key findings come from
719 these new dates: the previously unknown overlaps in volcanic activity between both the Silver
720 and Centre Hills and Centre and Soufrière Hills, and the discovery of a new, older stage of
721 Soufrière Hills activity ~450–290 ka with the eruption of hornblende-orthopyroxene lavas.

722 Combined with ages of volcanic centers on Basse-Terre, Guadeloupe, our ages suggest that
723 ~0.5–1 Ma is a common lifespan for volcanic centers in the Lesser Antilles. Furthermore,
724 overlap in activity between closely spaced (<10 km) volcanic centers on the same island appears
725 to be a common phenomenon in island arcs, as it has been observed on multiple islands in the
726 Lesser Antilles and Izu-Bonin-Mariana arcs.

727 **12. Acknowledgments**

728 We thank Adam Stinton and Rod Stewart for support during fieldwork, Agnes Michalik, Andy
729 Milton and Matt Cooper for assistance with geochemical analyses, and Jim Imlach for support
730 with $^{40}\text{Ar}/^{39}\text{Ar}$ sample preparation. We also thank Jack Palmer and Josh Brown for assistance
731 with hand picking samples for $^{40}\text{Ar}/^{39}\text{Ar}$ dating. Brian Jicha and an anomalous reviewer are
732 thanked for their comments, which helped improve this manuscript. $^{40}\text{Ar}/^{39}\text{Ar}$ dates were funded
733 by NERC Isotope Geosciences Facility allocation IP-1537-0515. We also acknowledge funding
734 from NERC IODP Case studentship NE/K007386/1. Supporting information has been provided
735 in Text S1–2, Figures S1–3, and Tables S1–4.

736 **13. References**

- 737 Andreastuti, S.D., Alloway, B. V., Smith, I.E.M., 2000. A detailed tephrostratigraphic
738 framework at Merapi Volcano, Central Java, Indonesia: implications for eruption
739 predictions and hazard assessment. *J. Volcanol. Geotherm. Res.* 100, 51–67.
740 doi:10.1016/S0377-0273(00)00133-5
- 741 Baker, P.E., 1985. Volcanic hazards on St Kitts and Montserrat, West Indies. *J. Geol. Soc.*
742 London 142, 279–295. doi:10.1130/MEM164-p169
- 743 Baker, P.E., 1984. Geochemical evolution of St Kitts and Montserrat, Lesser Antilles. *J. Geol.*
744 *Soc. London.* 141, 401–411. doi:10.1144/gsjgs.141.3.0401
- 745 Baker, P.E., Buckley, F., Padfield, T., 1980. Petrology of the volcanic rocks of Saba, West
746 Indies. *Bull. Volcanol.* 43, 337–346. doi:10.1007/BF02598037
- 747 Barclay, J., Alexander, J., Sušnik, J., 2007. Rainfall-induced lahars in the Belham Valley,
748 Montserrat, West Indies. *J. Geol. Soc. London.* 164, 815–827. doi:10.1144/0016-76492006-
749 078
- 750 Barclay, J., Rutherford, M.J., Carroll, M.R., Murphy, M.D., Devine, J.D., Gardner, J., Sparks,
751 R.S.J., 1998. Experimental phase equilibria constraints on pre-eruptive storage conditions of
752 the Soufrière Hills magma. *Geophys. Res. Lett.* 25, 3437. doi:10.1029/98GL00856
- 753 Bennett, E.H.S., Rose, W.I., Conway, F.M., 1992. Santa María, Guatemala: A decade volcano.
754 *Eos, Trans. Am. Geophys. Union* 73, 521–522. doi:10.1029/91EO00387
- 755 Boudon, G., Balcone-Boissard, H., Solaro, C., Martel, C., 2017. Revised chronostratigraphy of
756 recurrent ignimbritic eruptions in Dominica (Lesser Antilles arc): Implications on the
757 behavior of the magma plumbing system. *J. Volcanol. Geotherm. Res.* 343, 135–154.

758 doi:10.1016/j.jvolgeores.2017.06.022

759 Brown, K., Davidson, C., 2008. $^{40}\text{Ar}/^{39}\text{Ar}$ geochronology of the Silver Hills andesite,
760 Montserrat, West Indies. B. A. Sr. Integr. Exerc. Carlton College, Northfield, Minnesota.

761 Caricchi, L., Annen, C., Blundy, J., Simpson, G., Pinel, V., 2014. Frequency and magnitude of
762 volcanic eruptions controlled by magma injection and buoyancy. *Nat. Geosci.* 7, 126–130.
763 doi:10.1038/ngeo2041

764 Carlut, J., Quidelleur, X., Courtillot, V., Boudon, G., 2000. Paleomagnetic directions and K/Ar
765 dating of 0 to 1 Ma lava flows from La Guadeloupe Island Implications for time-averaged
766 field models. *J. Geophys. Res.* 105, 835–849.

767 Cassidy, M., Taylor, R.N., Palmer, M.R., Cooper, R.J., Stenlake, C., Trofimovs, J., 2012.
768 Tracking the magmatic evolution of island arc volcanism: Insights from a high-precision Pb
769 isotope record of Montserrat, Lesser Antilles. *Geochemistry, Geophys. Geosystems* 13, 1–
770 19. doi:10.1029/2012GC004064

771 Cassidy, M., Trofimovs, J., Watt, S.F.L., Palmer, M.R., Taylor, R.N., Gernon, T.M., Talling,
772 P.J., Le Friant, A., 2014. Multi-stage collapse events in the South Soufrière Hills,
773 Montserrat as recorded in marine sediment cores. *Geol. Soc. London, Mem.* 39, 383–397.
774 doi:10.1144/M39.20

775 Christopher, T.E., Humphreys, M.C.S., Barclay, J., Genareau, K., De Angelis, S.M.H., Plail, M.,
776 Donovan, A., 2014. Petrological and geochemical variation during the Soufrière Hills
777 eruption, 1995 to 2010. *Geol. Soc. London, Mem.* 39, 317–342. doi:10.1144/M39.17

778 Cole, P.D., Calder, E.S., Sparks, R.S.J., Clarke, A.B., Druitt, T.H., Young, S.R., Herd, R.A.,
779 Harford, C.L., Norton, G.E., 2002. Deposits from dome-collapse and fountain-collapse

780 pyroclastic flows at Soufrière Hills Volcano, Montserrat. *Geol. Soc. London, Mem.* 21,
781 231–262. doi:10.1144/GSL.MEM.2002.021.01.11

782 Cole, P.D., Smith, P.J., Stinton, A.J., Odbert, H.M., Bernstein, M.L., Komorowski, J.C., Stewart,
783 R., 2014. Vulcanian explosions at Soufrière Hills Volcano, Montserrat between 2008 and
784 2010. *Geol. Soc. London, Mem.* 39, 93–111. doi:10.1144/M39.5

785 Coussens, M., Cassidy, M., Watt, S.F.L., Jutzeler, M., Talling, P.J., Barfod, D., Gernon, T.M.,
786 Taylor, R., Hatter, S.J., Palmer, M.R., 2017. Long-term changes in explosive and effusive
787 behaviour at andesitic arc volcanoes: Chronostratigraphy of the Centre Hills Volcano,
788 Montserrat. *J. Volcanol. Geotherm. Res.* doi:10.1016/j.jvolgeores.2017.01.003

789 Coussens, M., Wall-Palmer, D., Talling, P.J., Watt, S.F.L., Cassidy, M., Jutzeler, M., Clare,
790 M.A., Hunt, J.E., Manga, M., Gernon, T.M., Palmer, M.R., Hatter, S.J., Boudon, G., Endo,
791 D., Fujinawa, A., Hatfield, R., Hornbach, M.J., Ishizuka, O., Kataoka, K., Le Friant, A.,
792 Maeno, F., McCanta, M., Stinton, A.J., 2016. The relationship between eruptive activity,
793 flank collapse, and sea level at volcanic islands: A long-term (>1 Ma) record offshore
794 Montserrat, Lesser Antilles. *Geochemistry, Geophys. Geosystems* 17, 2591–2611.
795 doi:doi:10.1002/2015GC006053.

796 Crandell, D.R., Miller, C.D., Glicken, H.X., Christiansen, R.L., Newhall, C.G., 1984.
797 Catastrophic debris avalanche from ancestral Mount Shasta volcano, California. *Geology*
798 12, 143–146. doi:10.1130/0091-7613(1984)12<143:CDAFAM>2.0.CO;2

799 Davidson, J., Wilson, M., 2011. Differentiation and source processes at Mt Pelée and the Quill;
800 Active volcanoes in the Lesser Antilles arc. *J. Petrol.* 52, 1493–1531.
801 doi:10.1093/petrology/egq095

802 Defant, M.J., Sherman, S., Maury, R.C., Bellon, H., De Boer, J., Davidson, J., Kepezhinskas, P.,
803 2001. The geology, petrology, and petrogenesis of Saba Island, Lesser Antilles. *J. Volcanol.*
804 *Geotherm. Res.* 107, 87–111. doi:10.1016/S0377-0273(00)00268-7

805 Deplus, C., Friant, A. Le, Boudon, G., Komorowski, J.C., Villemant, B., Harford, C., Segoufin,
806 J., Cheminee, J.L., 2001. Submarine evidence for large-scale debris avalanches in the Lesser
807 Antilles arc. *Earth Planet. Sci. Lett.* 192, 145–157.

808 Devine, J.D., Murphy, M.D., Rutherford, M.J., Barclay, J., Sparks, R.S.J., Carroll, M.R., Young,
809 S.R., Gardner, J.E., 1998. Petrologic evidence for pre-eruptive pressure-temperature
810 conditions, and recent reheating, of andesitic magma erupting at the Soufrière Hills
811 Volcano, Montserrat, W.I. *Geophys. Res. Lett.* 25, 3669–3672. doi:10.1029/98GL01330

812 Devine, J.D., Rutherford, M.J., Norton, G.E., Young, S.R., 2003. Magma Storage Region
813 Processes Inferred from Geochemistry of Fe–Ti Oxides in Andesitic Magma, Soufrière
814 Hills Volcano, Montserrat, W.I. *J. Petrol.* 44, 1375–1400. doi:10.1093/petrology/44.8.1375

815 Elliott, T., Plank, T., Zindler, A., White, W., Bourdon, B., 1997. Element transport from slab to
816 volcanic front at the Mariana arc. *J. Geophys. Res.* 102, 14991–15019.

817 Ewart, A., Collerson, K.D., Regelous, M., Wendt, J.I., Niu, Y., 1998. Geochemical Evolution
818 within the Tonga- Kermadec-Lau Arc-Back-arc Systems : the Role of Varying Mantle
819 Wedge Composition in Space and Time. *J. Petrol.* 39, 331–368. doi:10.1093/etroj/39.3.331

820 Expedition 340 scientists, T., 2013. Site U1396, in: Le Friant, A., Ishizuka, O., Stroncik, N.A.,
821 Expedition 340 scientists, T. (Eds.), *Proceedings of the Integrated Ocean Drilling Program,*
822 *340. Integrated Ocean Drilling Program Management Internation, Inc, Tokyo.*
823 doi:10.2204/iodp.proc.340.106.2013

824 Fraass, A.J., Wall-Palmer, D., Leckie, R.M., Hatfield, R.G., Burns, S.J., Le Friant, A., Ishizuka,
825 O., Aljahdali, M., Jutzeler, M., Martinez-Colon, M., Palmer, M.R., Talling, P.J., 2016. A
826 revised Plio-Pleistocene age model and paleoceanography of the northeastern Caribbean
827 Sea: IODP Site U1396 off Montserrat, Lesser Antilles. *Stratigraphy* 13, 183–203.

828 Germa, A., Quidelleur, X., Labanieh, S., Chauvel, C., Lahitte, P., 2011a. The volcanic evolution
829 of Martinique Island: Insights from K-Ar dating into the Lesser Antilles arc migration since
830 the Oligocene. *J. Volcanol. Geotherm. Res.* 208, 122–135.
831 doi:10.1016/j.jvolgeores.2011.09.007

832 Germa, A., Quidelleur, X., Labanieh, S., Lahitte, P., Chauvel, C., 2010. The eruptive history of
833 Morne Jacob volcano (Martinique Island, French West Indies): Geochronology,
834 geomorphology and geochemistry of the earliest volcanism in the recent Lesser Antilles arc.
835 *J. Volcanol. Geotherm. Res.* 198, 297–310. doi:10.1016/j.jvolgeores.2010.09.013

836 Germa, A., Quidelleur, X., Lahitte, P., Labanieh, S., Chauvel, C., 2011b. The K-Ar Cassagnol-
837 Gillot technique applied to western Martinique lavas: A record of Lesser Antilles arc
838 activity from 2 Ma to Mount Pelée volcanism. *Quat. Geochronol.* 6, 341–355.
839 doi:10.1016/j.quageo.2011.02.001

840 Glicken, H., 1996. Rockslide-debris avalanche of may 18, 1980, Mount St. Helens volcano,
841 Washington. Open-file Rep. 96-677 1–5.

842 Hall, P.S., Kincaid, C., 2001. Diapiric Flow at Subduction Zones: A Recipe for Rapid Transport.
843 *Science* (80-.). 292, 2472–2475. doi:10.1126/science.1060488

844 Harford, C.L., Pringle, M.S., Sparks, R.S.J., Young, S.R., 2002. The volcanic evolution of
845 Montserrat using $^{40}\text{Ar}/^{39}\text{Ar}$ geochronology. *Geol. Soc. London, Mem.* 21, 93–113.

846 doi:10.1144/GSL.MEM.2002.021.01.05

847 Hart, S.R., 1984. A large-scale isotope anomaly in the Southern Hemisphere mantle. *Nature* 309,
848 753–757.

849 Hatfield, R.G., 2015. Data report: stratigraphic correlation of Site U1396 and creation of a
850 composite depth scale and splice 340, 1–17. doi:10.2204/iodp.proc.340.202.2015

851 Hildreth, W., Drake, R.E., 1992. Volcán Quizapu, Chilean Andes. *Bull. Volcanol.* 54, 93–125.

852 Hildreth, W., Lanphere, M.A., 1994. Potassium-argon geochronology of a basalt-andesite-dacite
853 arc system: The Mount Adams volcanic field, Cascade Range of southern Washington.
854 *Geol. Soc. Am. Bull.* 106, 1413–1429. doi:10.1130/0016-
855 7606(1994)106<1413:PAGOAB>2.3.CO;2

856 Hoblitt, R.P., Crandell, D.R., Mullineaux, D.R., 1980. Mount St . Helens eruptive behavior
857 during the past 1 , 500 yr. *Geology* 8, 555–559. doi:10.1130/0091-7613(1980)8<555

858 Hoshizumi, H., Uto, K., Watanabe, K., 1999. Geology and eruptive history of Unzen volcano,
859 Shimabara Peninsula, Kyushu, SW Japan. *J. Volcanol. Geotherm. Res.* 89, 81–94.

860 Howe, T.M., Lindsay, J.M., Shane, P., 2015. Evolution of young andesitic-dacitic magmatic
861 systems beneath Dominica, Lesser Antilles. *J. Volcanol. Geotherm. Res.* 297, 69–88.

862 Ishizuka, O., Geshi, N., Itoh, J., Kawanabe, Y., TuZino, T., 2008. The magmatic plumbing of the
863 submarine Hachijo NW volcanic chain, Hachijojima, Japan: Long-distance magma
864 transport? *J. Geophys. Res. Solid Earth* 113. doi:10.1029/2007JB005325

865 Ishizuka, O., Taylor, R.N., Geshi, N., Oikawa, T., Kawanabe, Y., Ogitsu, I., 2015. Progressive
866 mixed-magma recharging of Izu-Oshima volcano, Japan: A guide to magma chamber
867 volume. *Earth Planet. Sci. Lett.* 430, 19–29. doi:10.1016/j.epsl.2015.08.004

868 Ishizuka, O., Taylor, R.N., Yuasa, M., Milton, J.A., Nesbitt, R.W., Uto, K., Sakamoto, I., 2007.
869 Processes controlling along-arc isotopic variation of the southern Izu-Bonin arc.
870 *Geochemistry, Geophys. Geosystems* 8. doi:10.1029/2006GC001475

871 Kamber, B.S., Gladu, A.H., 2009. Comparison of Pb Purification by Anion-Exchange Resin
872 Methods and Assessment of Long-Term Reproducibility of Th/U/Pb Ratio Measurements
873 by Quadrupole ICP-MS. *Geostand. Geoanalytical Res.* 33, 169–181. doi:10.1111/j.1751-
874 908X.2009.00911.x

875 Kokelaar, B.P., 2002. Setting, chronology and consequences of the eruption of Soufrière Hills
876 Volcano, Montserrat (1995-1999). *Erupt. Soufrière Hills Volcano, Montserrat, from 1995 to*
877 *1999* 21, 1–43. doi:10.1144/GSL.MEM.2002.021.01.02

878 Koleszar, A.M., Kent, A.J.R., Wallace, P.J., Scott, W.E., 2012. Controls on long-term low
879 explosivity at andesitic arc volcanoes: Insights from Mount Hood, Oregon. *J. Volcanol.*
880 *Geotherm. Res.* 219–220, 1–14. doi:10.1016/j.jvolgeores.2012.01.003

881 Komorowski, J.C., Boudon, G., Smet, M., Beauducel, F., Antenor-Habazac, C., Bazin, S.,
882 Hammouya, G., 2005. Guadeloupe, in: Unit, S.R. (Ed.), *Volcanic Hazard Atlas of the*
883 *Lesser Antilles*. University of the West Indies, St Augustine, Trinidad, W.I., pp. 67–104.

884 Labanieh, S., Chauvel, C., Germa, A., Quidelleur, X., 2012. Martinique: A clear case for
885 sediment melting and slab dehydration as a function of distance to the trench. *J. Petrol.* 53,
886 2441–2464. doi:10.1093/petrology/egs055

887 Labanieh, S., Chauvel, C., Germa, A., Quidelleur, X., Lewin, E., 2010. Isotopic hyperbolas
888 constrain sources and processes under the Lesser Antilles arc. *Earth Planet. Sci. Lett.* 298,
889 35–46. doi:10.1016/j.epsl.2010.07.018

890 Le Friant, A., Harford, C.L., Deplus, C., Boudon, G., Sparks, R.S.J., Herd, R. a., Komorowski,
891 J.C., 2004. Geomorphological evolution of Montserrat (West Indies): importance of flank
892 collapse and erosional processes. *J. Geol. Soc. London.* 161, 147–160. doi:10.1144/0016-
893 764903-017

894 Le Friant, A., Lock, E.J., Hart, M.B., Boudon, G., Sparks, R.S.J., Leng, M., Smart, C.W.,
895 Komorowski, J.-C., Deplus, C., Fisher, J.K., 2008. Late Pleistocene tephrochronology of
896 marine sediments adjacent to Montserrat, Lesser Antilles volcanic arc. *J. Geol. Soc.*
897 *London.* 165, 279–289. doi:10.1144/0016-76492007-019

898 Lebas, E., Le Friant, A., Boudon, G., Watt, S.F.L., Talling, P.J., Feuillet, N., Deplus, C., Berndt,
899 C., Vardy, M.E., 2011. Multiple widespread landslides during the long-term evolution of a
900 volcanic island: Insights from high-resolution seismic data, Montserrat, Lesser Antilles.
901 *Geochemistry, Geophys. Geosystems* 12. doi:10.1029/2010GC003451

902 Lindsay, J.M., Trumbull, R.B., Siebel, W., 2005. Geochemistry and petrogenesis of late
903 Pleistocene to Recent volcanism in Southern Dominica, Lesser Antilles. *J. Volcanol.*
904 *Geotherm. Res.* 148, 253–294. doi:10.1016/j.jvolgeores.2005.04.018

905 Macdonald, R., Hawkesworth, C.J., Heath, E., 2000. The Lesser Antilles volcanic chain: A study
906 in arc magmatism. *Earth Sci. Rev.* 49, 1–76. doi:10.1016/S0012-8252(99)00069-0

907 Macgregor, A.G., 1938. The Royal Society Expedition to Montserrat, B.W.I. The Volcanic
908 History and Petrology of Montserrat, with Observations on Mt Pelée, in Martinique. *Philos.*
909 *Trans. R. Soc. Lond. B. Biol. Sci.* 229, 1–90.

910 Mark, D.F., Barfod, D., Stuart, F.M., Imlach, J., 2009. The ARGUS multicollector noble gas
911 mass spectrometer: Performance for $^{40}\text{Ar}/^{39}\text{Ar}$ geochronology. *Geochemistry, Geophys.*

912 Geosystems 10, n/a-n/a. doi:10.1029/2009GC002643

913 Marske, J.P., Pietruszka, A.J., Trusdell, F.A., Garcia, M.O., 2011. Geochemistry of southern
914 Pagan Island lavas, Mariana arc: The role of subduction zone processes. *Contrib. to*
915 *Mineral. Petrol.* 162, 231–252. doi:10.1007/s00410-010-0592-1

916 Maury, R.C., Westbrook, G.K., Baker, P.E., Bouysse, P., Westercamp, D., 1990. Geology of the
917 Lesser Antilles, in: Dengo, G., Case, J.E. (Eds.), *The Geology of North America, Vol. H,*
918 *The Caribbean Region.* Geological Society of America, Boulder, Colorado, pp. 141–166.

919 Miller, T.P., Chertkoff, D.G., Eichelberger, J.C., Coombs, M.L., 1999. Mount Dutton volcano,
920 Alaska: Aleutian arc analog to Unzen volcano, Japan. *J. Volcanol. Geotherm. Res.* 89, 275–
921 301. doi:10.1016/S0377-0273(99)00004-9

922 Minster, J.B., Jordan, T.H., 1978. Present-day plate motions. *J. Geophys. Res.* 83, 5331.
923 doi:10.1029/JB083iB11p05331

924 Murphy, M.D., Sparks, R.S.J., Barclay, J., Carroll, M.R., Brewer, T.S., 2000. Remobilization of
925 Andesite Magma by Intrusion of Mafic Magma at the Soufrière Hills Volcano, Montserrat,
926 West Indies. *J. Petrol.* 41, 21–42. doi:10.1093/petrology/41.1.21

927 Murphy, M.D., Sparks, R.S.J., Barclay, J., Carroll, M.R., Lejeune, A.M., Brewer, T.S.,
928 Macdonald, R., Black, S., Young, S., 1998. The role of magma mixing in triggering the
929 current eruption of the Soufrière Hills volcano, Montserrat, West Indies. *Geophys. Res.*
930 *Lett.* 25, 3433–3436.

931 Myers, J.D., Marsh, B.D., Sinha, A.K., 1985. Strontium isotopic and select trace element
932 variations between two Aleutian volcanic centres (Adak and Atka): Implications for the
933 development of arc volcanic plumbing systems. *Contrib. to Mineral. Petrol.* 91, 221–234.

934 Odbert, H.M., Ryan, G.A., Mattioli, G.S., Hautmann, S., Gottsmann, J., Fournier, N., Herd, R.A.,
935 2014. Volcano geodesy at the Soufrière Hills Volcano, Montserrat: a review, in: Wadge, G.,
936 Robertson, R.E.A., Voight, B. (Eds.), *The Eruption of Soufrière Hills Volcano, Montserrat*
937 *from 2000 to 2010*. Geological Society, London, *Memoirs*, pp. 195–217.
938 doi:10.1144/M39.11

939 Palmer, M.R., Hatter, S.J., Gernon, T.M., Taylor, R.N., Cassidy, M., Johnson, P., Le Friant, A.,
940 Ishizuka, O., 2016. Discovery of a large 2.4 Ma Plinian eruption of Basse-Terre,
941 Guadeloupe, from the marine sediment record. *Geol.* 44, 123–126. doi:10.1130/G37193.1

942 Pinel, V., Jaupart, C., Albino, F., 2010. On the relationship between cycles of eruptive activity
943 and growth of a volcanic edifice. *J. Volcanol. Geotherm. Res.* 194, 150–164.
944 doi:10.1016/j.jvolgeores.2010.05.006

945 Pioli, L., Scalisi, L., Costantini, L., Di Muro, A., Bonadonna, C., Clavero, J., 2015. Explosive
946 style, magma degassing and evolution in the Chaimilla eruption, Villarrica volcano,
947 Southern Andes. *Bull. Volcanol.* 77. doi:10.1007/s00445-015-0976-1

948 Plail, M., Barclay, J., Humphreys, M.C.S., Edmonds, M., Herd, R.A., Christopher, T.E., 2014.
949 Characterization of mafic enclaves in the erupted products of Soufrière Hills Volcano,
950 Montserrat, 2009 to 2010. *Geol. Soc. London, Mem.* 39, 343–360. doi:10.1144/M39.18

951 Rea, W.J., 1974. The volcanic geology and petrology of Montserrat, West Indies. *J. Geol. Soc.*
952 *London.* 130, 341–366. doi:10.1144/gsjgs.130.4.0341

953 Renne, P.R., Balco, G., Ludwig, K.R., Mundil, R., Min, K., 2011. Response to the comment by
954 W.H. Schwarz et al. on “Joint determination of 40K decay constants and $40\text{Ar}^*/40\text{K}$ for the
955 Fish Canyon sanidine standard, and improved accuracy for $40\text{Ar}/39\text{Ar}$ geochronology” by

- 956 P. R. Renne et al. (2010). *Geochim. Cosmochim. Acta* 75, 5097–5100.
957 doi:10.1016/j.gca.2011.06.021
- 958 Renne, P.R., Mundil, R., Balco, G., Min, K., Ludwig, K.R., 2010. Joint determination of ^{40}K
959 decay constants and $^{40}\text{Ar}^*/^{40}\text{K}$ for the Fish Canyon sanidine standard, and improved
960 accuracy for $^{40}\text{Ar}/^{39}\text{Ar}$ geochronology. *Geochim. Cosmochim. Acta* 74, 5349–5367.
961 doi:10.1016/j.gca.2010.06.017
- 962 Ricci, J., Lahitte, P., Quidelleur, X., 2015a. Construction and destruction rates of volcanoes
963 within tropical environment: Examples from the Basse-Terre Island (Guadeloupe, Lesser
964 Antilles). *Geomorphology* 228, 597–607. doi:10.1016/j.geomorph.2014.10.002
- 965 Ricci, J., Quidelleur, X., Lahitte, P., 2015b. Volcanic evolution of central Basse-Terre Island
966 revisited on the basis of new geochronology and geomorphology data. *Bull. Volcanol.* 77,
967 84. doi:10.1007/s00445-015-0970-7
- 968 Ridolfi, F., Renzulli, A., Puerini, M., 2010. Stability and chemical equilibrium of amphibole in
969 calc-alkaline magmas: An overview, new thermobarometric formulations and application to
970 subduction-related volcanoes. *Contrib. to Mineral. Petrol.* doi:10.1007/s00410-009-0465-7
- 971 Roobol, M.J., Smith, A.L., 1998. Pyroclastic stratigraphy of the Soufrière Hills volcano,
972 Montserrat - Implications for the present eruption. *Geophys. Res. Lett.* 25, 3393–3396.
- 973 Roobol, M.J., Smith, A.L., 1976. Mount Pelée, Martinique: A pattern of alternating eruptive
974 styles. *Geology* 4, 521–524. doi:10.1130/0091-7613(1976)4<521:MPMAPO>2.0.CO;2
- 975 Rose, W.I., 1987. Santa María, Guatemala: bimodal soda-rich calc-alkalic stratovolcano. *J.*
976 *Volcanol. Geotherm. Res.* 33, 109–129.
- 977 Rose, W.I., 1973. Pattern and mechanism of volcanic activity at the Santiaguito Volcanic Dome,

978 Guatemala. Bull. Volcanol. 37, 73–94. doi:10.1007/BF02596881

979 Rose, W.I., 1972. Santiaguito Volcanic Dome, Guatemala. Geol. Soc. Am. Bull. 83, 1413–1434.

980 Rowley, K., 1978. Late Pleistocene pyroclastic deposits of Soufrière Volcano, St. Vincent, West
981 Indies. Bull. Geol. Soc. Am. 89, 825–835. doi:10.1130/0016-
982 7606(1978)89<825:LPPDOS>2.0.CO;2

983 Ruprecht, P., Bachmann, O., 2010. Pre-eruptive reheating during magma mixing at Quizapu
984 volcano and the implications for the explosiveness of silicic arc volcanoes. Geology 38,
985 919–922. doi:10.1130/G31110.1

986 Samper, A., Quidelleur, X., Komorowski, J.-C., Lahitte, P., Boudon, G., 2009. Effusive history
987 of the Grande Découverte Volcanic Complex, southern Basse-Terre (Guadeloupe, French
988 West Indies) from new K–Ar Cassignol–Gillot ages. J. Volcanol. Geotherm. Res. 187, 117–
989 130. doi:10.1016/j.jvolgeores.2009.08.016

990 Samper, A., Quidelleur, X., Lahitte, P., Mollex, D., 2007. Timing of effusive volcanism and
991 collapse events within an oceanic arc island: Basse-Terre, Guadeloupe archipelago (Lesser
992 Antilles Arc). Earth Planet. Sci. Lett. 258, 175–191. doi:10.1016/j.epsl.2007.03.030

993 Scott, W.E., Pierson, T.C., Schilling, S.P., Costa, J.E., Gardner, C.A., Vallance, J.W., Major, J.J.,
994 1997. Volcano Hazards in the Mount Hood Region, Oregon. US Geol. Surv. Open-File Rep.
995 1–14.

996 Siebert, L., 1984. Large volcanic debris avalanches: Characteristics of source areas, deposits, and
997 associated eruptions. J. Volcanol. Geotherm. Res. 22, 163–197. doi:10.1016/0377-
998 0273(84)90002-7

999 Smith, A.L., Roobol, M.J., Mattioli, G.S., Fryxell, J.E., Daly, G.E., Fernandez, L.A., 2013. The

1000 volcanic geology of the mid-arc island of Dominica, Lesser Antilles: The surface expression
1001 of a island-arc batholith. Geological Society of America, Boulder, Colorado.

1002 Smith, A.L., Roobol, M.J., Schellekens, J.H., Mattioli, G.S., 2007. Prehistoric stratigraphy of the
1003 Soufrière Hills - South Soufrière Hills volcanic complex, Montserrat, West Indies. *Geology*
1004 115, 115–127.

1005 Sparks, R.S.J., Barclay, J., Calder, E.S., Herd, R. a., Komorowski, J.-C., Luckett, R., Norton,
1006 G.E., Ritchie, L.J., Voight, B., Woods, a. W., 2002. Generation of a debris avalanche and
1007 violent pyroclastic density current on 26 December (Boxing Day) 1997 at Soufrière Hills
1008 Volcano, Montserrat. *Geol. Soc. London, Mem.* 21, 409–434.
1009 doi:10.1144/GSL.MEM.2002.021.01.18

1010 Sparks, R.S.J., Folkes, C.B., Humphreys, M.C.S., Barfod, D.N., Clavero, J., Sunagua, M.C.,
1011 McNutt, S.R., Pritchard, M.E., 2008. Uturuncu volcano, Bolivia: Volcanic unrest due to
1012 mid-crustal magma intrusion. *Am. J. Sci.* 308, 727–769. doi:10.2475/06.2008.01

1013 Stern, R.J., 2002. Subduction zones. *Rev. Geophys.* 40. doi:10.1029/2001RG000108

1014 Stinton, A.J., Cole, P.D., Stewart, R.C., Odbert, H.M., Smith, P., 2014. The 11 February 2010
1015 partial dome collapse at Soufrière Hills Volcano, Montserrat. *Geol. Soc. London, Mem.* 39,
1016 133–152. doi:10.1144/M39.7

1017 Takarada, S., Ui, T., Yamamoto, Y., 1999. Depositional features and transportation mechanism
1018 of valley-filling Iwasegawa and Kaida debris avalanches, Japan. *Bull. Volcanol.* 60, 508–
1019 522. doi:10.1007/s004450050248

1020 Taylor, R.N., Ishizuka, O., Michalik, A., Milton, J.A., Croudace, I.W., 2015. Evaluating the
1021 precision of Pb isotope measurement by mass spectrometry. *J. Anal. At. Spectrom.* 30, 198–

1022 213. doi:10.1039/C4JA00279B

1023 Toothill, J., Williams, C. a., MacDonald, R., Turner, S.P., Rogers, N.W., Hawkesworth, C.J.,
1024 Jerram, D. a., Ottley, C.J., Tindle, a. G., 2007. A complex petrogenesis for an arc magmatic
1025 suite, St Kitts, Lesser Antilles. *J. Petrol.* 48, 3–42. doi:10.1093/petrology/egl052

1026 Ui, T., 1983. Volcanic dry avalanche deposits — Identification and comparison with nonvolcanic
1027 debris stream deposits. *J. Volcanol. Geotherm. Res.* 18, 135–150.
1028 doi:10.1016/j.jvolgeores.2008.06.025

1029 Ui, T., Glicken, H., 1986. Internal structural variations in a debris-avalanche deposit from
1030 ancestral Mount Shasta, California, USA. *Bull. Volcanol.* 48, 189–194.
1031 doi:10.1007/BF01087673

1032 Ui, T., Kawachi, S., Neall, V.E., 1986. Fragmentation of debris avalanche material during
1033 flowage — Evidence from the Pungarehu Formation, Mount Egmont, New Zealand. *J.*
1034 *Volcanol. Geotherm. Res.* 27, 255–264. doi:10.1016/0377-0273(86)90016-8

1035 van Wyk de Vries, B., Davies, T., 2015. Landslides, Debris Avalanches and Volcanic
1036 Gravitational Deformation, in: Sigurdsson, H., Houghton, B., McNutt, S.R., Rymer, H.,
1037 Stix, J. (Eds.), *Encyclopedia of Volcanoes*. Elsevier Inc., pp. 665–685.

1038 Venezky, D.Y., Rutherford, M.J., 1999. Petrology and Fe–Ti oxide reequilibration of the 1991
1039 Mount Unzen mixed magma. *J. Volcanol. Geotherm. Res.* 213–230.

1040 Voight, B., Komorowski, J.-C., Norton, G.E., Belousov, A.B., Belousova, M., Boudon, G.,
1041 Francis, P.W., Franz, W., Heinrich, P., Sparks, R.S.J., Young, S.R., 2002. The 26 December
1042 (Boxing Day) 1997 sector collapse and debris avalanche at Soufrière Hills Volcano,
1043 Montserrat. *Geol. Soc. London, Mem.* 21, 363–407.

- 1044 doi:10.1144/GSL.MEM.2002.021.01.17
- 1045 Wadge, G., Voight, B., Sparks, R.S.J., Cole, P.D., Loughlin, S.C., Robertson, R.E.A., 2014. An
1046 overview of the eruption of Soufrière Hills Volcano, Montserrat from 2000 to 2010. *Geol.*
1047 *Soc. London, Mem.* 39, 1–40. doi:10.1144/M39.1
- 1048 Wendt, I., Carl, C., 1991. The statistical distribution of the mean squared weighted deviation.
1049 *Chem. Geol. Isot. Geosci. Sect.* 86, 275–285. doi:10.1016/0168-9622(91)90010-T
- 1050 Westercamp, D., Traineau, H., 1983. The past 5,000 years of volcanic activity at Mt. Pelée
1051 Martinique (F.W.I): Implications for assessment of volcanic hazards. *J. Volcanol.*
1052 *Geotherm. Res.* 17, 159–185.
- 1053 White, J.D.L., Houghton, B.F., 2006. Primary volcanoclastic rocks. *Geology* 34, 677–680.
1054 doi:10.1130/G22346.1
- 1055 Wohletz, K., Heiken, G., Ander, M., Goff, F., Vuataz, F.-D., Wadge, G., 1986. The Qualibou
1056 caldera, St. Lucia, West Indies. *J. Volcanol. Geotherm. Res.* 27, 77–115.
- 1057 Wright, J. V., Roobol, M.J., Smith, A.L., Sparks, R.S.J., Brazier, S.A., Rose, W.I., Sigurdsson,
1058 H., 1984. Late Quaternary explosive silicic volcanism on St Lucia, West Indies. *Geol. Mag.*
1059 121, 1–15. doi:10.1017/S0016756800027904
- 1060 Young, S.R., Hoblitt, R.P., Smith, A.L., Devine, J.D., Wadge, G., Shepherd, J.B., 1996. Dating
1061 of explosive volcanic eruptions associated with dome growth at the Soufrière Hills volcano,
1062 Montserrat, West Indies, in: *Second Caribbean Conference on Natural Hazards and Hazard*
1063 *Management.*

1064

1065 **Figure Captions**

1066 Figure 1: (a) Map of Montserrat with bathymetry (100 m intervals), showing the location of the
1067 volcanic centers and $^{40}\text{Ar}/^{39}\text{Ar}$ dates. Pale areas with horizontal stripes are uplifted regions.
1068 Orange areas with diagonal stripes within the Soufrière Hills show the locations of the lava
1069 domes: 1, Chances Peak; 2, Gages Mountain; 3, Galway's Mountain; 4, Perches Mountain; 5,
1070 Castle Peak. Dot-dashed line shows edge of English's Crater. White dots mark the locations of
1071 Soufrières, which are (from left to right): Gages Lower, Gages Upper, Galway's and Tar River.
1072 Accepted ages in bold. Ages viewed with caution: ^m maximum age; ^r Ar recoil; ^x excess Ar; ^e
1073 MSWD exceeds critical value; see text for details. (b) Map of the Lesser Antilles, showing the
1074 location of IODP Expedition 340 core site U1396.

1075 Figure 2: Exposure map of Silver Hills with locations of $^{40}\text{Ar}/^{39}\text{Ar}$ dates and stratigraphic logs.
1076 Accepted ages in bold. Ages viewed with caution: ^m maximum age; ^e MSWD exceeds critical
1077 value; ⁿ age from non-reproducible release spectra; see text for details. Contour spacing is 100
1078 feet. Bold contours are every 500 feet. British West Indies Grid; each grid square is 1 km².

1079 Figure 3: Plateau age diagrams for the twelve lava samples. Ages in Ma $\pm 2\sigma$.

1080 Figure 4: Age-probability spectra for the three pumice samples. Dotted lines show spectra
1081 including all data, solid lines show spectra after data rejection. Data at 1 σ , results at 2 σ , ages in
1082 Ma $\pm 2\sigma$. Includes error in J. Filtering: nMAD = 1.5.

1083 Figure 5: (a) Sketch of exposure along north Marguerita Bay, showing the relationship between
1084 units. Heavy black line = joint. (b) Southern corner of the exposure shown in (a), showing unit
1085 MB8 (left) cutting down through units MB3–4 (right). (c) Interdigitation of units MB4 and
1086 MB5. (d) Mingled boundary between units MB8 (grey) and MB9 (golden brown), with isolated
1087 blocks of MB8 floating in MB9. See supplementary material for unit descriptions.

1088 Figure 6: (a) Stratigraphic log from log site 1 at the top of Potato Hill. Units PH2 and 4 are the
1089 poorly-sorted sub-facies, unit PH3 is well-sorted sub-facies. (b) Stratigraphic logs from log sites
1090 2 (left) and 3 (right) in Old Quaw Ghaut. Note the significant variation between the two sites,
1091 just ~60 m apart. Black clasts represent andesite, orange clasts hydrothermally altered andesite,
1092 white clasts pumice.

1093 Figure 7: Pb isotopes showing separation between the South Soufrière Hills, Soufrière Hills and
1094 Centre and Silver Hills. $\Delta_{7/4}$ is $^{207}\text{Pb}/^{204}\text{Pb}$ calculated to the Northern Hemisphere Reference
1095 Line (Hart, 1984).

1096 Figure 8. Nb/Y vs $^{143}\text{Nd}/^{144}\text{Nd}$ separating between Silver and Centre Hills. (a) Terrestrial
1097 samples, and identifying the provenance of samples with uncertain origin: SMB, South
1098 Marguerita Bay; LKB, Lime Kiln Bay; DH, Davy Hill; PH, Potato Hill. (b) marine tephra
1099 samples from core U1396C. Numbers note age of tephra layers in Ma. Faded terrestrial samples
1100 are shown for comparison.

1101 Figure 9: Thin section images of andesite lava and enclave textures, and boundaries between
1102 them.

1103 Figure 10: Schematic map-view evolution of the Silver Hills volcanic center. Active domes and
1104 their associated deposits are in bold.

1105 Figure 11: Timing of volcanic activity on Montserrat. Colored bands define our revised timings
1106 of volcanism for the different volcanic centers. All literature ages are shown for comparison.
1107 Literature ages from Harford et al. (2002); Brown and Davidson, (2008); Coussens et al. (2017).

1108 Figure S1: Block-and-ash flow deposits (units V2–4) by Valentine Hill.

1109 Figure S2: (a) Highly fractured andesite lava, east of Potato Hill, which is locally brecciated (b).
1110 Notebook for scale is 19 x 12 cm.

1111 Figure S3: (a) Field sketch of a road cutting at GR 378001 1856419 (road to Davy Hill) showing
1112 a pyroclastic sequence (units DH1–4) filling a channel in hydrothermally altered lava. Facing
1113 SSW. (b) Single-unit volcanoclastic megablock of stratified tuff, and (c) sheared single-unit
1114 volcanoclastic megablocks of tuff, within unit DH5 (highlighted by black lines).

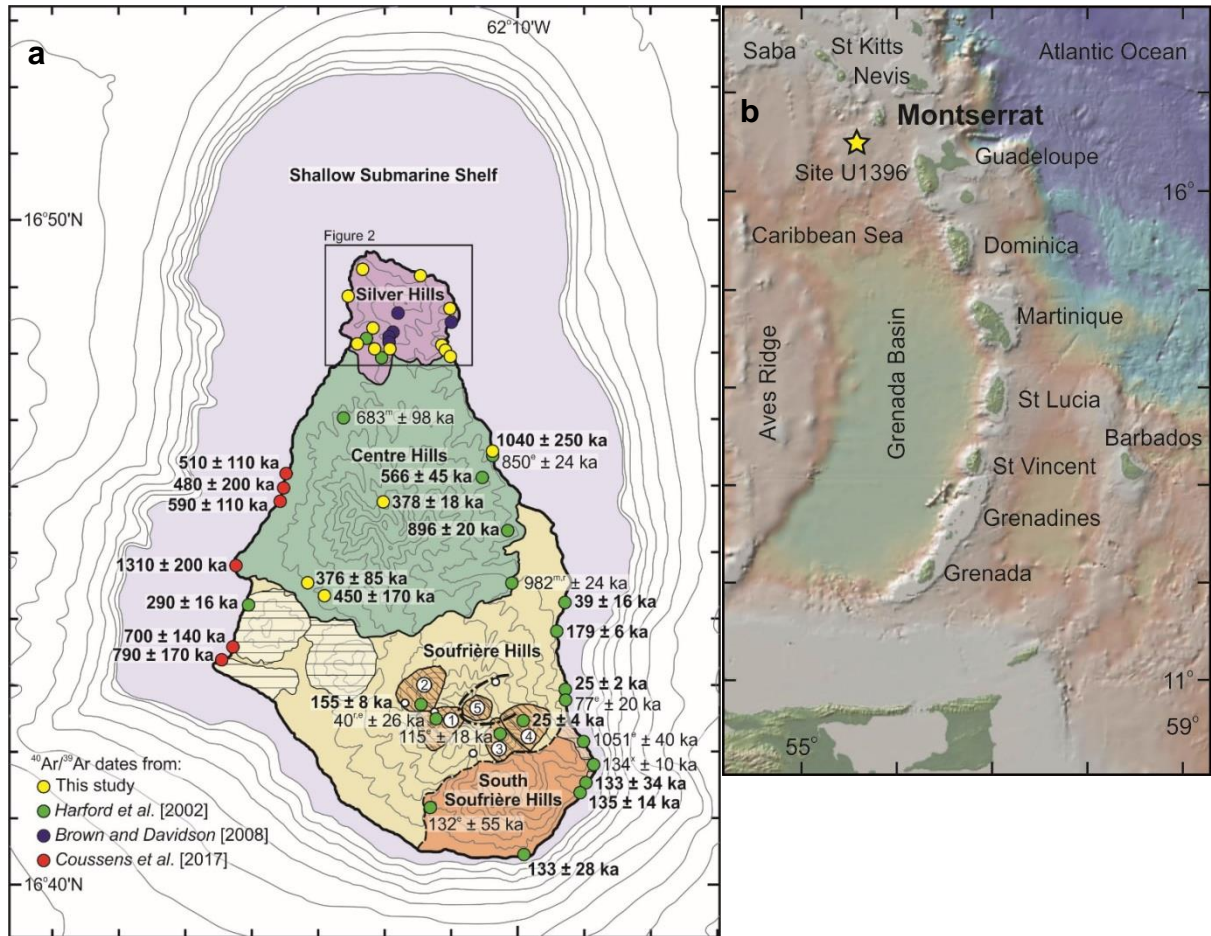
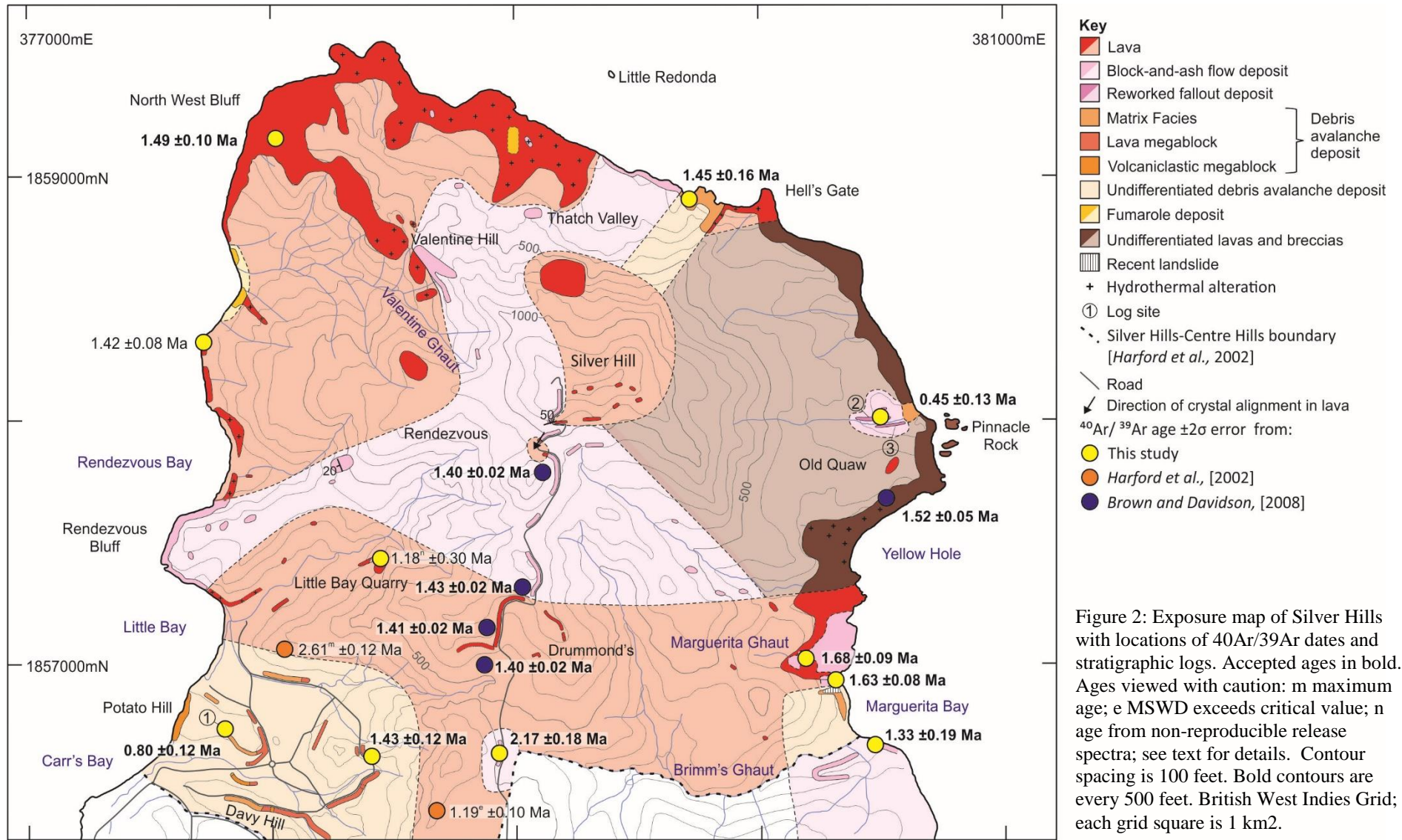


Figure 1: (a) Map of Montserrat with bathymetry (100 m intervals), showing the location of the volcanic centers and $^{40}\text{Ar}/^{39}\text{Ar}$ dates. Pale areas with horizontal stripes are uplifted regions. Orange areas with diagonal stripes within the Soufrière Hills show the locations of the lava domes: 1, Chances Peak; 2, Gages Mountain; 3, Galway's Mountain; 4, Perches Mountain; 5, Castle Peak. Dot-dashed line shows edge of English's Crater. White dots mark the locations of Soufrières, which are (from left to right): Gages Lower, Gages Upper, Galway's and Tar River. Accepted ages in bold. Ages viewed with caution: ^m maximum age; ^r Ar recoil; ^x excess Ar; ^e MSWD exceeds critical value; see text for details. (b) Map of the Lesser Antilles, showing the location of IODP Expedition 340 core site U1396.



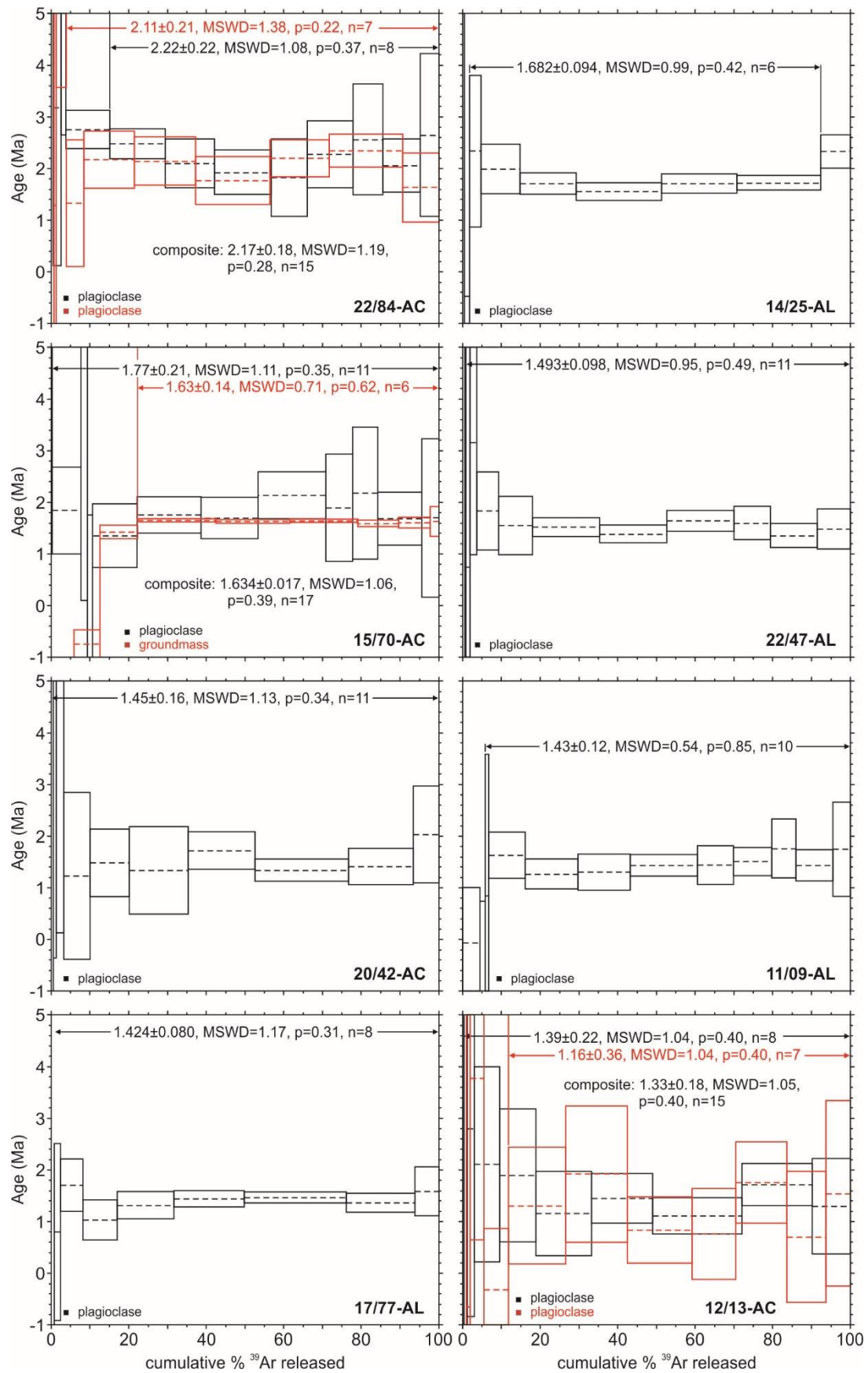


Figure 3: Plateau age diagrams for the twelve lava samples. Ages in $\text{Ma} \pm 2\sigma$.

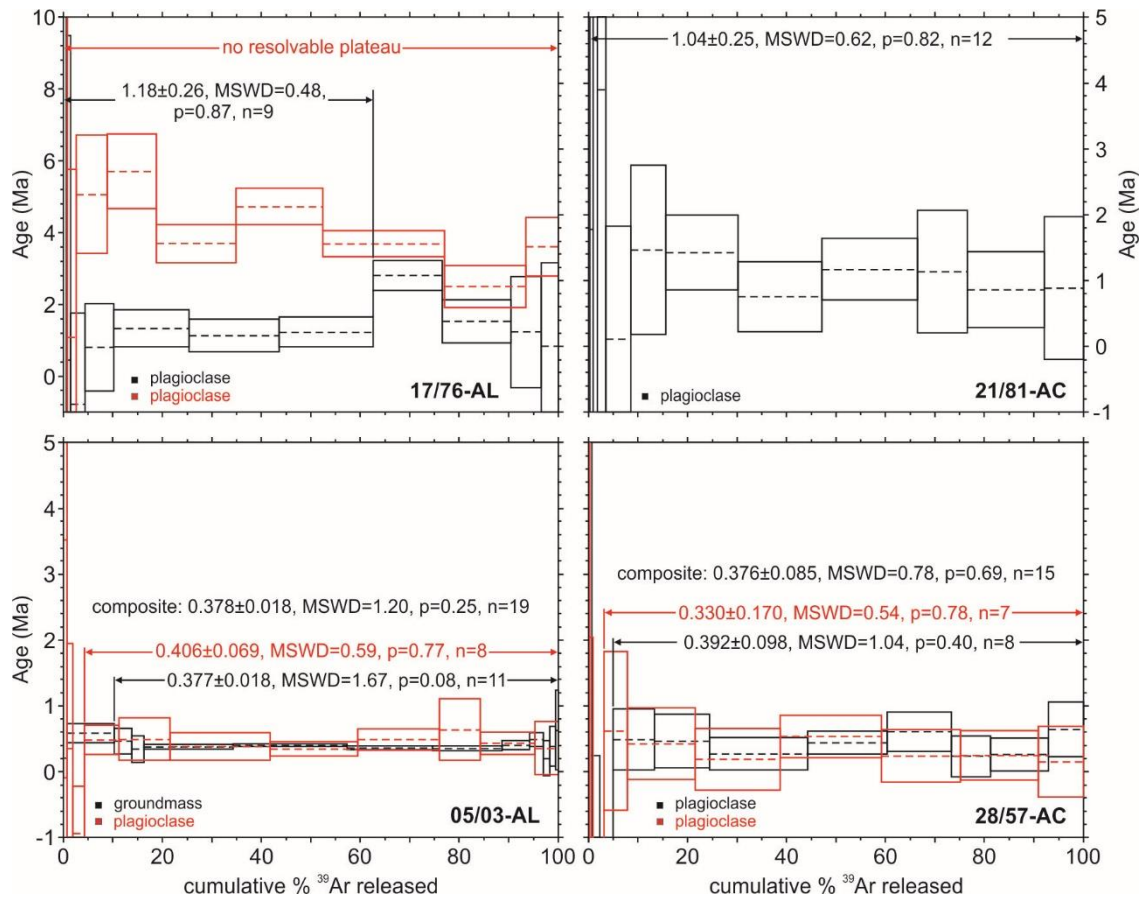


Figure 3 continued

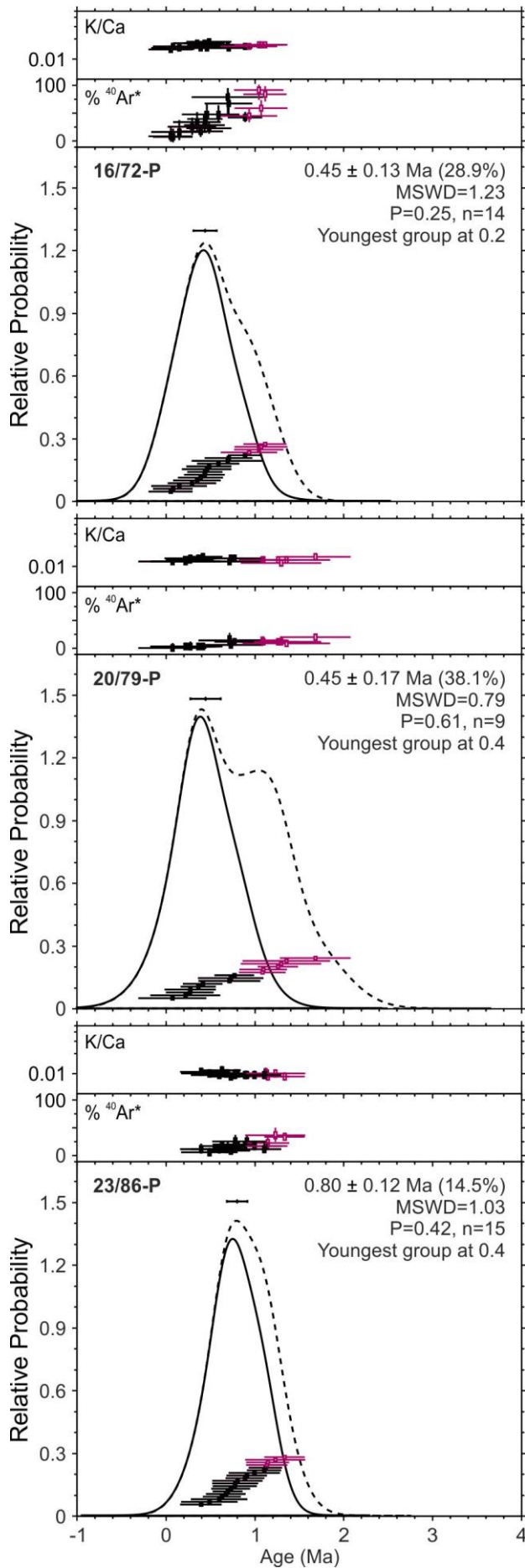


Figure 4: Age-probability spectra for the three pumice samples. Dotted lines show spectra including all data, solid lines show spectra after data rejection. Ages in $\text{Ma} \pm 2\sigma$.

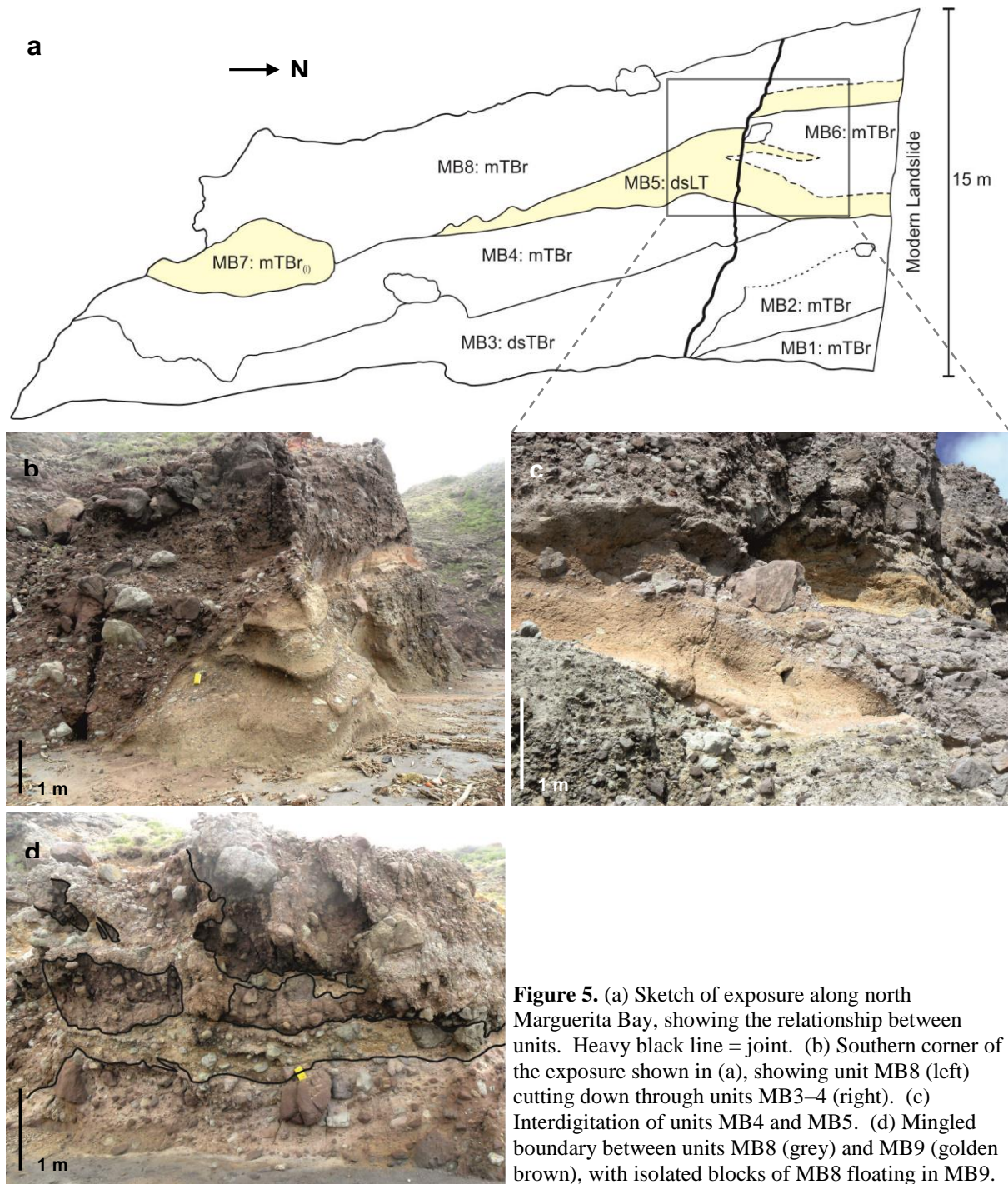


Figure 5. (a) Sketch of exposure along north Marguerita Bay, showing the relationship between units. Heavy black line = joint. (b) Southern corner of the exposure shown in (a), showing unit MB8 (left) cutting down through units MB3–4 (right). (c) Interdigitation of units MB4 and MB5. (d) Mingled boundary between units MB8 (grey) and MB9 (golden brown), with isolated blocks of MB8 floating in MB9.

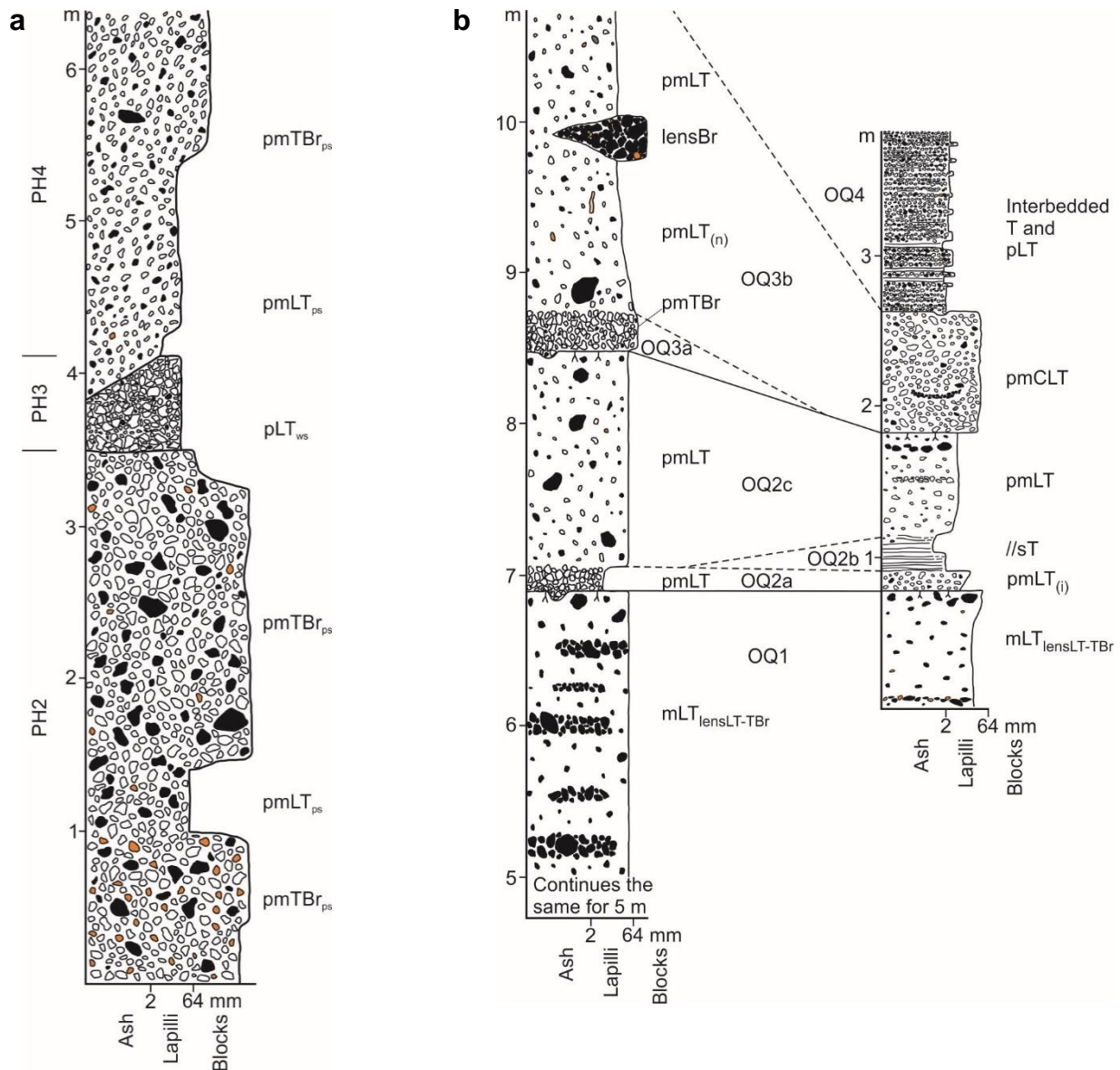


Figure 6. (a) Stratigraphic log from log site 1 at the top of Potato Hill. Units PH2 and 4 are the poorly-sorted sub-facies, unit PH3 is well-sorted sub-facies. (b) Stratigraphic logs from log sites 2 (left) and 3 (right) in Old Quaw Ghaut. Note the significant variation between the two sites, just ~60 m apart. Black clasts represent andesite, orange clasts hydrothermally altered andesite, white clasts pumice.

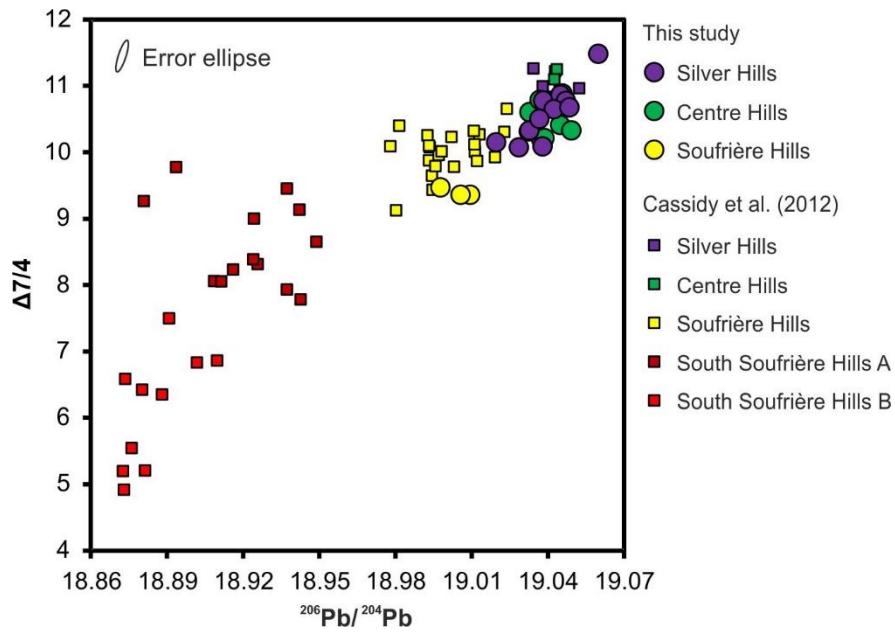


Figure 7. Pb isotopes showing separation between the South Soufrière Hills, Soufrière Hills and Centre and Silver Hills. $\Delta 7/4$ is $^{207}\text{Pb}/^{204}\text{Pb}$ calculated to the Northern Hemisphere Reference Line [Hart, 1984].

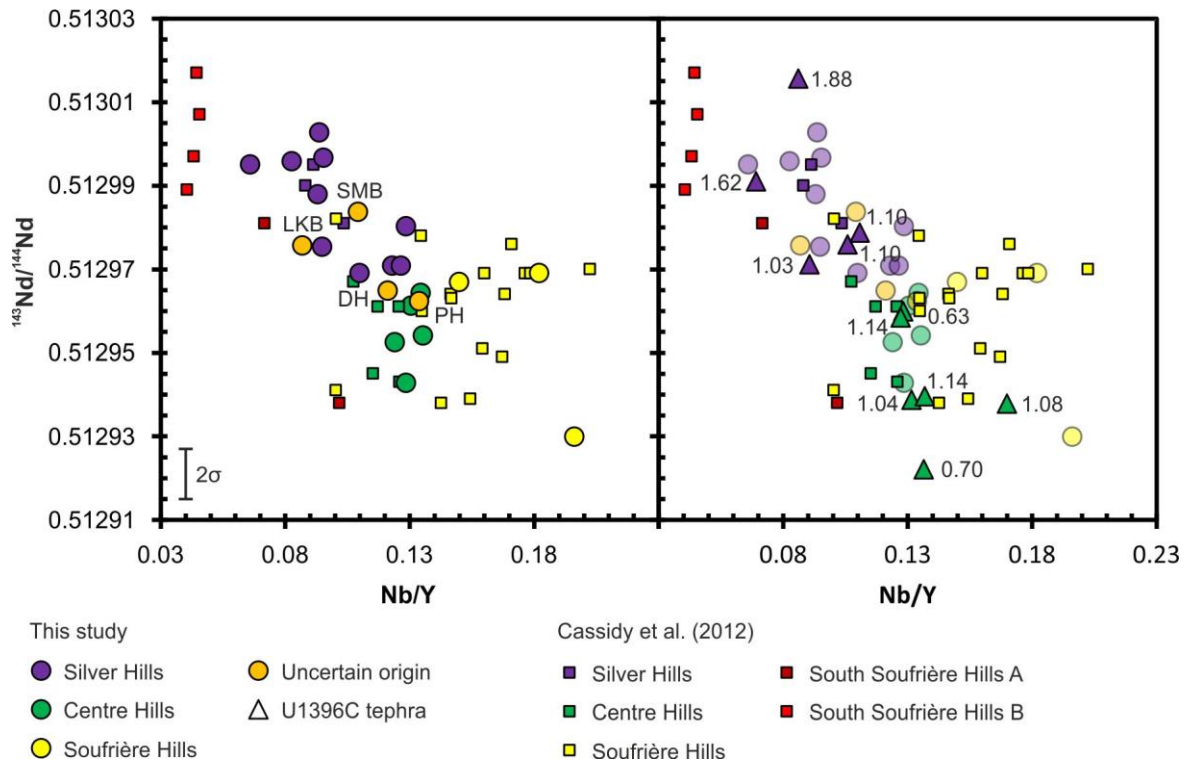


Figure 8. Nb/Y vs $^{143}\text{Nd}/^{144}\text{Nd}$ separating between Silver and Centre Hills. (a) Terrestrial samples, and identifying the provenance of samples with uncertain origin: SMB, South Marguerita Bay; LKB, Lime Kiln Bay; DH, Davy Hill; PH, Potato Hill. (b) marine tephra samples from core U1396C. Numbers note age of tephra layers in Ma. Faded terrestrial samples are shown for comparison.

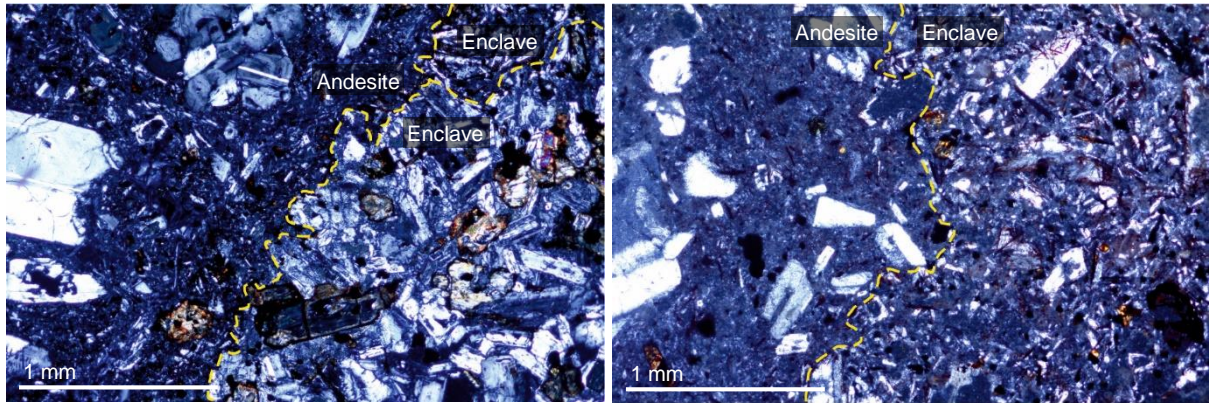
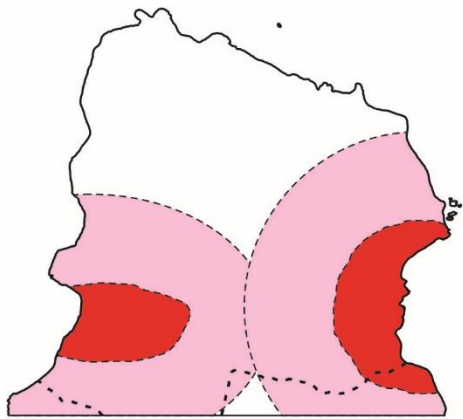
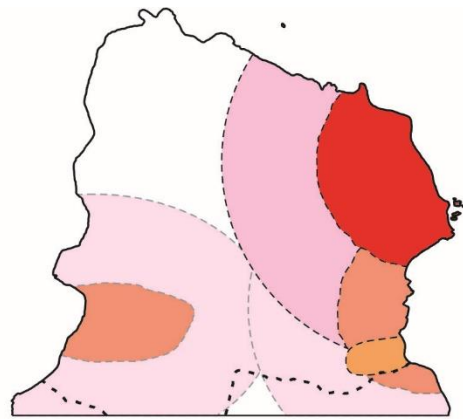


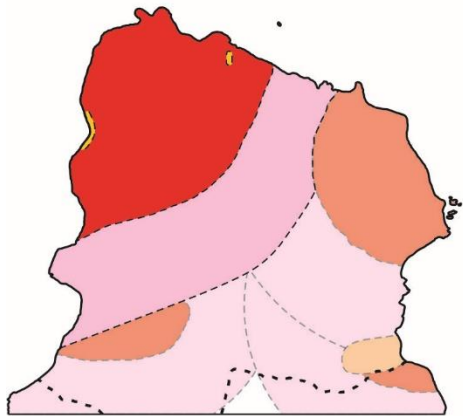
Figure 9. Thin section images of andesite lava and enclave textures, and boundaries between them.



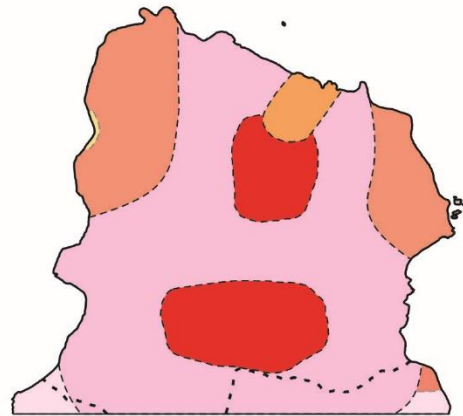
~2.17 Ma: Little Bay | 1.7–1.6 Ma: Marguerita Bay



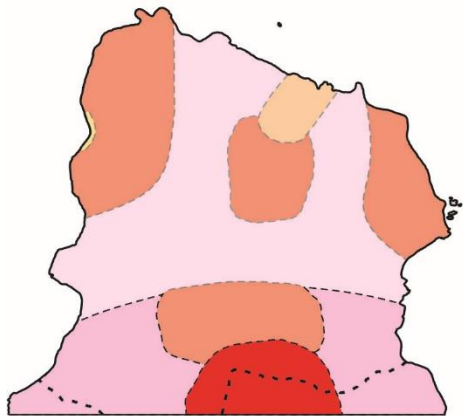
1.5 Ma: Yellow Hole



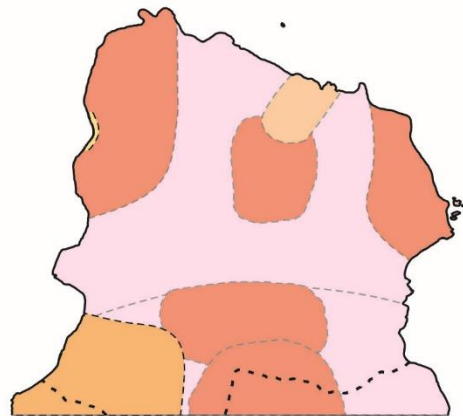
1.5–1.4 Ma: Northwest Bluff



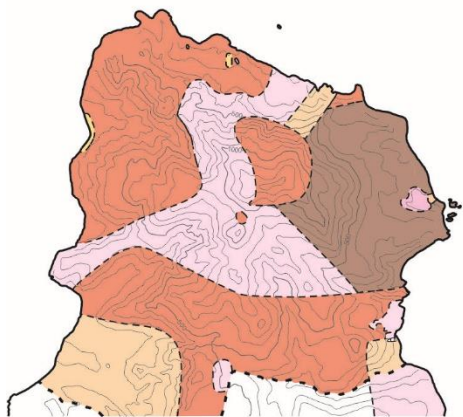
1.4 Ma: Silver Hill and Drummonds



1.3 Ma: South Drummonds



~1.0–0.8 Ma: Little Bay debris avalanche



Present Day

Key








-  Lava
-  Block-and-ash flow deposit
-  Reworked fallout deposit
-  Undifferentiated debris avalanche deposit
-  Fumarole deposit
-  Undifferentiated lavas and breccias
-  Recent landslide

Figure 10. Schematic map-view evolution of the Silver Hills volcanic center. Active domes and their associated deposits are in bold.

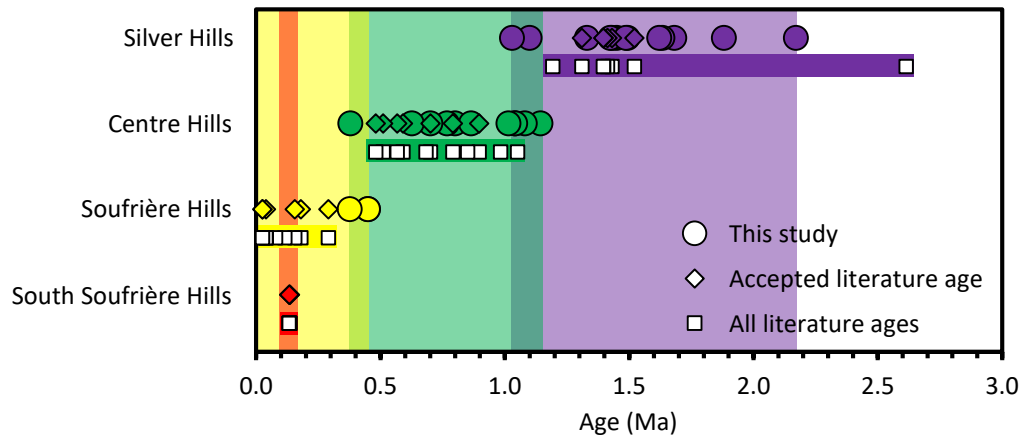


Figure 11. Timing of volcanic activity on Montserrat. Colored bands define our revised timings of volcanism for the different volcanic centers. All literature ages are shown for comparison. Literature ages from Harford et al., [2002]; Brown and Davidson, [2008]; Coussens et al., [2017].

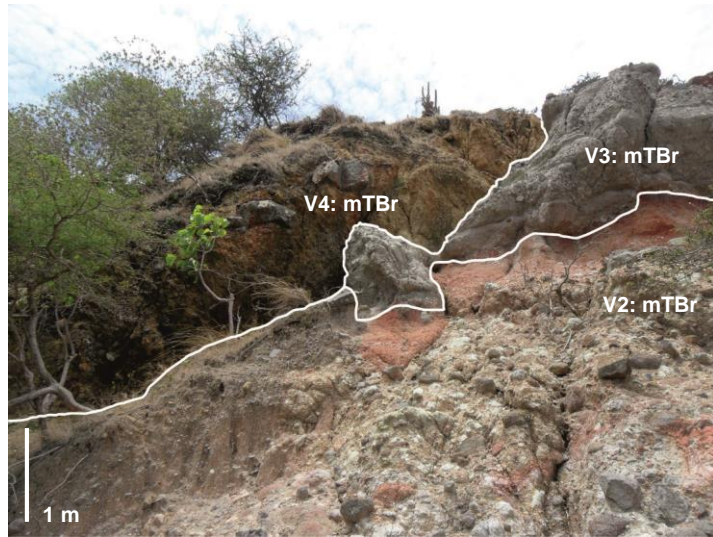


Figure S1. Block-and-ash flow deposits (units V2–4) by Valentine Hill.

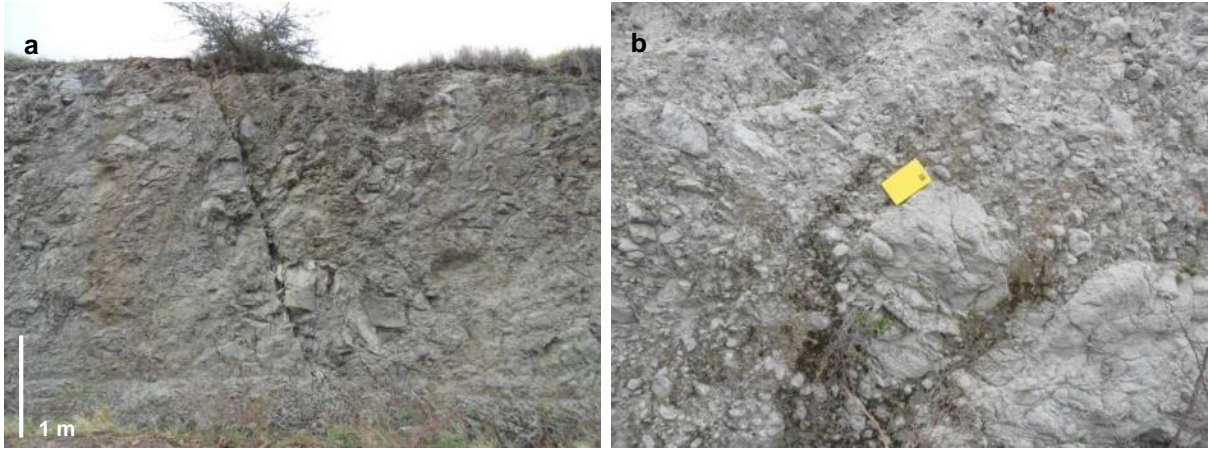


Figure S2. (a) Highly fractured andesite lava, east of Potato Hill, which is locally brecciated (b). Notebook for scale is 19 x 12 cm.

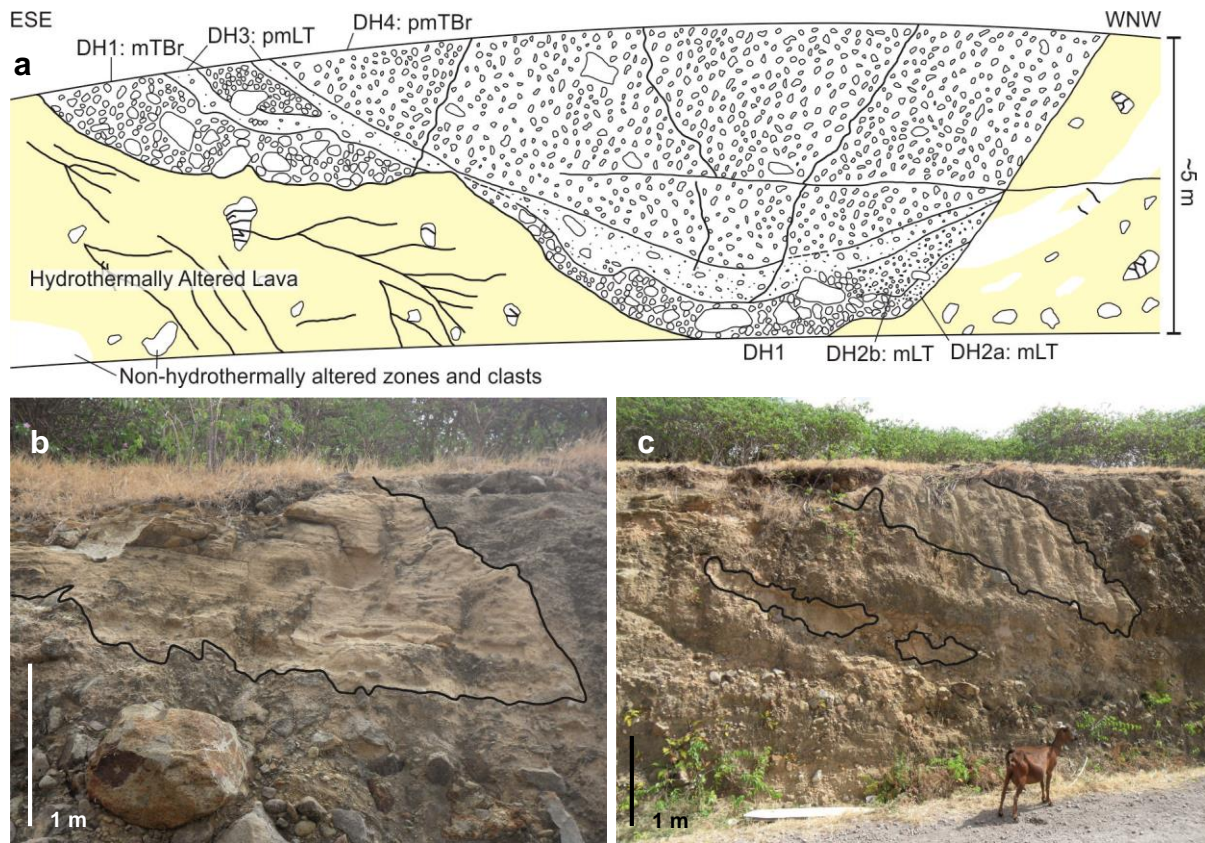


Figure S3. (a) Field sketch of a road cutting at GR 378001 1856419 (road to Davy Hill) showing a pyroclastic sequence (units DH1–4) filling a channel in hydrothermally altered lava. Facing SSW. (b) Single-unit volcanoclastic megablock of stratified tuff, and (c) sheared single-unit volcanoclastic megablocks of tuff, within unit DH5 (highlighted by black lines).

Table 1. Compiled literature $^{40}\text{Ar}/^{39}\text{Ar}$ dates on Montserrat. Ages from Harford et al., (2002) and Brown and Davidson, (2008) presented here are recalculated ages (see text for details).

Sample	Rock type	Location/unit	Grid reference mE mN	Material	Plateau age (ka)	$\pm 2\sigma$	MSWD	N	% ^{39}Ar
MVO144 ¹	Lava	Silver Hill	378025 1857050	Plagioclase	2614 ^m	121	0.69	7/11	65.3
SH07-F ²	Lava	Yellow Hole	380408 1857634	Groundmass	1520ⁱ	51	0.58	7/7	100.0
SH07-C ²	Lava	Drummonds	379033 1857296	Groundmass	1430ⁱ	19	1.09	7/7	100.0
SH07-D ²	BAF	Drummonds	378873 1857117	Groundmass	1412ⁱ	20	0.66	7/8	>95.0
SH07-B ²	BAF	Silver Hill	379081 1857776	Groundmass	1397ⁱ	20	0.46	7/7	100.0
SH07-E ²	Lava	Drummonds	378859 1857000	Groundmass	1395ⁱ	17	0.82	7/7	100.0
11.1.4C ³	PAF	South Lime Kiln Bay	374681 1851092	Plagioclase	1310	200	0.95	6/7	
MVO755 ¹	Lava	Silver Hill	378650 1856400	Groundmass	1192 ^f	95	20.79 ^e	5/16	64.6
MVO135 ¹	s-BAF	Roche's Bluff	383975 1846150	Whole-rock	1051	40	4.37 ^e	7/14	62.1
MOV148 ¹	Lava	Harris	382150 1850450	Whole-rock	982 ^{m,r}	24	4.99 ^e	10/12	93.0
MVO131 ¹	Lava	Trant's	382050 1851975	Whole-rock	896	20	1.40	12/12	100.0
MVO831 ¹	BAF	Lower Centre Hills	381763 1853525	Groundmass	850	24	2.01 ^e	9/14	73.7
BP ³	PF	Bransby Pumice	374092 1848396	Plagioclase	790	170	0.87	6/7	
4.2.3G ³	PAF	Old Road Bay	374638 1848989	Plagioclase	700	140	0.88	5/6	
MVO147 ¹	PAF	Upper Centre Hills	377600 1855050	Plagioclase	683 ^m	98	0.93	5/12	76.4
3.1.2A ³	PAF	Woodlands Bay	375879 1852755	Plagioclase	590	110	1.14	7/7	100.0
MVO809 ¹	BAF	Upper Centre Hills	381475 1853750	Groundmass	566	45	1.01	14/14	100.0
3.4.2H ³	PAF	Bunkum Bay	376014 1853421	Plagioclase	510	110	0.41	5/7	
3.1.8C ³	PAF	Attic	375951 1853042	Plagioclase	480	200	0.99	3/8	
MVO785 ¹	BAF	Garibaldi Hill	374990 1850025	Groundmass	290	16	0.15	6/15	66.7
MVO819 ¹	—	SH-1 ⁴	383238 1849275	Groundmass	182	10	2.48 ^e	5/10	91.5
				Groundmass	178	6	1.03	5/9	66.7
				Composite	179	6	0.53		
MVO152 ¹	Lava	Gages Dome	379275 1847175	Whole-rock	230	14	0.23	5/14	53.6
				Groundmass	163	12	3.23	2/10	53.7
				Groundmass	153	6	1.06	5/9	64.2
				Composite	155	8	1.84		
MVO139 ¹	Lava	Landing Bay	383950 1845000	Whole-rock	142	18	1.28	5/11	61.1
				Groundmass	128	18	2.89 ^e	14/17	87.1
				Composite	135	14	1.13		
MVO136 ¹	Lava	Roche's Bluff	384250 1845650	Whole-rock	134 ^{l,x}	10	0.79	10/11	97.4
MVO830 ¹	Breccia	Roche's Bluff	383975 1845050	Groundmass	133	34	0.64	8/16	76.0
MVO791 ¹	Lava	Shoe Rock	381600 1843150	Groundmass	133	28	0.35	6/10	70.7
MVO1099 ¹	—	SSH-F ⁴	379750 1844325	Groundmass	157	18	1.00	6/9	55.5
				Groundmass	102	20	0.45	3/9	63.0
				Composite	132	55	16.67 ^e		
18654 ¹	Lava	Galway's Dome	—	Groundmass	124	8	1.96	5/10	58.2
				Groundmass	106	10	0.52	4/10	59.4
				Composite	115	18	8.45 ^e		
MVO777 ¹	—	SH-II ⁴	383675 1847250	Groundmass	86	10	1.23	3/8	63.2
				Groundmass	66	12	0.33	3/9	60.4
				Composite	77	20	6.53 ^e		
MVO149 ¹	Lava	Chances Dome	379900 1846825	Whole-rock	40 ^f	26	15.9 ^e	4/11	54.2
MVO127 ¹	—	SH-III ⁴	383550 1849975	Groundmass	39	16	0.13	3/10	72.5
MVO154 ¹	Lava	Perches Dome	382100 1846750	Whole-rock	33	8	1.61	5/11	65.3
				Groundmass	25	4	0.54	5/9	65.9
				Groundmass	24	6	0.20	4/10	68.3
				Composite	25	4	0.18		

MVO775 ¹	—	SH-III ⁴	383425	1847675	Groundmass	25	2	0.93	4/9	64.0
MVO104 ¹	BAF	1996 Dome	—		Groundmass	22	44	0.25	4/10	63.8
					Plagioclase	439	192	3.26 ^e	7/10	71.1

¹ Harford et al., (2002); ² Brown and Davidson, (2008); ³ Coussens et al., (2017); ⁴ unit name from Smith et al., (2007). BAF, block-and-ash flow deposit; PAF, pumice-and-ash flow deposit; S-BAF, submarine-BAF; PF, pumice fall deposit. Ages considered reliable are in bold. Ages viewed with caution: ^m maximum age; ^r Ar recoil; ^x excess Ar; ^e MSWD exceeds critical value. ⁱ isochron age. N, number of plateau steps used to determine age/total number of steps; %³⁹Ar, percentage of total ³⁹Ar in N.

Table 2. New $^{40}\text{Ar}/^{39}\text{Ar}$ dates for the Silver Hills, Centre Hills and Soufrière Hills.

Sample	Rock type	Location/unit	Grid reference mE mN	Material	Isochron age (ka)	$\pm 2\sigma$	$^{40}\text{Ar}/^{36}\text{Ar}_{(i)}$	$\pm 2\sigma$	MS WD	Plateau age (ka)	$\pm 2\sigma$	MS WD	N	% ^{39}Ar	^{39}Ar (mol)	Ca/K	
22/84-AC	BAF	South Silver Hill	378940 1856619	Plagioclase	2160	200	300.6	8.4	1.20	2220	220	1.08	8/12	84.8	5.3E-17	105	
					Plagioclase	2300	630	290.0	23.0	1.50	2110	210	1.38	7/12	96.2	4.1E-17	99
					Composite	2140	260	299.5	8.0	1.30	2170	180	1.19	15/24		9.5E-17	103
14/25-AL	Lava	Marguerita Ghaut	380235 1857105	Plagioclase	1680	230	298.6	8.3	1.20	1682	94	0.99	6/10	90.5	8.4E-17	76	
15/70-AC	BAF	North Marguerita Bay	380310 1856978	Groundmass	1580	140	298.2	0.4	0.71	1630	140	0.71	6/12	77.6	6.6E-16	5	
					Plagioclase	1710	260	302.0	24.0	1.20	1770	210	1.11	11/12	99.6	6.1E-17	135
					Composite	1640	80	298.2	0.67	1.20	1634	83	1.06	17/24		7.2E-16	123
22/47-AL	Lava	North West Bluff	378130 1859071	Plagioclase	1550	130	293.0	13.0	0.97	1493	98	0.95	11/12	99.4	8.3E-17	79	
20/42-AC	MF	Thatch Valley	379710 1858870	Plagioclase	1340	140	302.2	3.8	1.20	1450	160	1.13	11/12	99.8	5.6E-17	107	
11/09-AL	LMB	Culture Hill	378378 1856630	Plagioclase	1510	180	296.5	30	0.49	1430	120	0.54	10/13	94.2	1.0E-16	64	
17/77-AL	Lava	North Rendezvous Bay	377754 1858327	Plagioclase	1260	330	305.0	12.0	1.00	1424	80	1.17	8/11	99.1	1.1E-16	54	
12/13-AC	BAF	South Marguerita Bay	380452 1856780	Plagioclase	1250	350	306.0	16.0	1.10	1390	220	1.04	8/10	98.9	3.7E-17	127	
					Plagioclase	1520	780	285.0	25.0	1.10	1160	360	1.04	7/12	88.3	2.0E-17	130
					Composite	1360	280	297.0	13.0	1.10	1330	190	1.05	15/22		5.7E-17	128
17/76-AL	Lava	Little Bay Quarry	378449 1857434	Plagioclase	Excess ^{40}Ar		No resolvable plateau										
					Plagioclase	1250	440	296.0	13.0	0.54	1180 ⁿ	300	0.50	9/13	62.6	3.0E-17	93
21/81-AC	BAF	East Centre Hills	381671 1853642	Plagioclase	1020	390	301.0	13.0	0.67	1040	250	0.62	12/12	100.0	5.3E-17	123	
05/03-AL	Lava	Dry Waterfall	378605 1852689	Groundmass	370	20	308.0	14.0	1.80	377	18	1.67	11/13	89.8	1.0E-15	6	
					Plagioclase	530	90	290.8	8.9	0.37	406	69	0.59	8/12	95.8	1.2E-16	54
					Composite	376	18	299.5	3.8	1.30	378	18	1.20	19/25		1.1E-15	53
28/57-AC	BAF	Spring Ghaut	376605 1850521	Plagioclase	400	140	298.3	3.7	1.20	392	98	1.04	8/11	95.0	7.3E-17	79	
					Plagioclase	240	340	300.4	4.8	0.53	330	170	0.54	7/10	96.9	5.2E-17	74
					Composite	360	110	298.9	2.1	0.84	376	85	0.78	15/21		1.2E-16	77
Pumice samples					Probability density Function Age (ka)												
23/86-PF	PF	Potato Hill	377806 1856742	Plagioclase						800	120	1.03	15/19			107	
20/79-PC	PAF	South Centre Hills	376612 1850198	Plagioclase						450	170	0.79	9/15			84	
16/72-PR	r-PF	Old Quaw Ghaut	380443 1857979	Plagioclase						450	130	1.23	14/18			66	

Abbreviations same as Table 2. MF, debris avalanche deposit matrix facies; LMB, lava megablock within debris avalanche deposit; r-PF, reworked-PF. Preferred ages for this study in bold. ⁿ age from non-reproducible release spectra. See supplementary Table 2 for decay rates, isotopic constants and nucleogenic production ratios.

Table 3. Lithofacies abbreviations used. Adapted from Branney and Kokelaar (2002). m-dsLT_{lensBr}, for example, means massive to diffuse-stratified lapilli-tuff with lenses of breccia.

Symbol	Lithofacies
T	Tuff
LT	Lapilli-tuff
TBr	Tuff-breccia
Br	Breccia
m	Massive
p	Pumice-rich
ds	Diffuse-stratified
//s	Parallel-stratified
(n)	Normal-graded
(i)	Inverse-graded
lensBr	Lens(es) of breccia
MB	Megablock

Table 4. Tephra layers in core U1396C spanning the time interval 2.35–0.37 Ma.

Tephra layer	Age (Ma)	Provenance	Pumice?*
2H1W-66/81	0.63	Centre Hills	Yes
2H2W-39.5/52	0.70	Centre Hills	Yes
2H2W-148.5/ 2H3W-14	0.77	Centre Hills	No
2H4W-94.5/98	0.86	Centre Hills	No
2H7W-62.5/67	1.02	Centre Hills	TF
3H1W-10/12	1.03	Silver Hills	Yes
3H1W-24/27.5	1.03	Guadeloupe	Yes
3H1W-50.5/53	1.04	Centre Hills	NVL
3H2W-23.5/26	1.08	Centre Hills	Yes
3H2W-58/67	1.10	Silver Hills	Yes
3H2W-142.5/149	1.14	Centre Hills	Yes
3H6-32/37	1.41	Guadeloupe	Yes
3H7W-33/40	1.49	Silver Hills	TF
4H2W-29/32	1.62	Silver Hills	Yes
4H6W-42/44	1.88	Silver Hills	Yes

*Contains enough pumice for geochemical analysis. TF, too fine-grained to separate pumice from the other components; NVL, fresh non-vesicular lava grains analysed.

